Table 1
Demographic characteristics of the subjects.

	Control	MCI non-converter	MCI converter	AD
N	12	7	6	15
Age (year)	67.3 ± 2.7	77.6 ± 3.1	80.2 ± 4.1	71.0 ± 5.1
Gender (F/M)	6/6	2/5	4/2	8/7
MMSE	29.9 ± 0.3	26.3 ± 1.1	25.7 ± 2.0	19.8 ± 3.5

of the subjects had asymptomatic cerebral infarction detected via T2-weighted MRI. Demographic data for the subjects are shown in Table 1. Although the MCI converters and non-converters were statistically older than the control subjects and the AD patients, no statistical difference in age was observed between the MCI converters and the non-converters. The AD patients showed a significantly lower MMSE score than the MCI converters, non-converters, and control subjects ($p<0.05$), however, no statistical difference in MMSE score was observed between the MCI converters and the non-converters. The Committee on Clinical Investigation at Tohoku University School of Medicine and the Advisory Committee on Radioactive Substances at Tohoku University approved the study protocol.

3. MRI methods

All subjects underwent MRI with a 1.5 T MR scanner (GE Signa Hispeed, Milwaukee, WI). A three-dimensional volumetric acquisition of a T1-weighted gradient echo sequence produced a gapless series of thin axial sections using a vascular TOF SPGR sequence (echo time/repetition time, 2.4/50 ms; flip angle, 45°; acquisition matrix, 256 × 256; 1 excitation; field of view, 22 cm; slice thickness, 2.0 mm). Cerebral atrophy was evaluated by VBM [41]. For spatial normalization, a 12-parameter affine transformation was used to avoid segmentation errors caused by the partial-volume effects inherently created by warping. The normalized MRI was then segmented into gray matter, white matter, cerebrospinal fluid, and other components using SPM2 or SPM5 software. The segmentation procedure involved calculating the Bayesian probability of each voxel belonging to each tissue class based on a priori MRI information with a non-uniformity correction. The segmented gray matter images were then subjected to affine and non-linear spatial normalization using a template of a priori gray matter. The spatially normalized gray matter images were smoothed with an isotropic Gaussian kernel (12 mm at full width at half maximum) using the partial-volume effects to create a spectrum of gray matter intensities. The resulting gray matter intensities were equivalent to the weighted average of gray matter voxels located in the volume fixed by the smoothing kernel. Regional intensities can thus be considered equivalent to gray matter concentration. Differences of gray matter intensities between groups were assessed using a *t*-test with a height threshold of $p<0.05$, corrected for multiple comparisons by the family-wise error method. The extent threshold was set to 100 voxels. Parahippocampal gray matter density was additionally evaluated by calculating the average intensities in the bilateral parahippocampal region of interest (ROI) using Dr.View/LINUX software (AJS, Japan). To evaluate global atrophy, a *Z*-score map was created via the comparison of individual gray matter images with the mean and S.D. of gray matter images of healthy controls after voxel normalization to global mean intensities. The degree of global atrophy (% global atrophy) was calculated as a ratio of the area in which the *Z*-score of the voxel was more than 2.0 to whole brain area, using Voxel-Based Specific Regional Analysis System for AD (VSRAD) software (Eisai, Tokyo, Japan) [42].

3.1. PET procedure

Radiosynthesis of [^{11}C]BF-227 and the procedure used for BF-227–PET were performed as described previously. [22] BF-227 and its N-desmethylated derivative (a precursor of [^{11}C]BF-227) were custom-synthesized by Tanabe R&D Service Co. [^{11}C]BF-227 was synthesized from its precursor by N-methylation in dimethyl sulfoxide using [^{11}C]methyl triflate. The [^{11}C]BF-227–PET study was performed using a PET SET-2400W scanner (Shimadzu Inc., Japan). After an intravenous injection of 211–366 mBq [^{11}C]BF-227, dynamic PET images were obtained for 60 min with the subject's eyes closed. Standardized uptake value (SUV) images of [^{11}C]BF-227 were obtained by normalizing the tissue radioactivity concentration to the injected dose and body weight. ROIs were placed on individual axial MR images in the cerebellar hemisphere and the frontal, lateral temporal, parietal and posterior cingulate cortices. The ROI information was then copied onto the dynamic PET SUV images, and regional SUVs were sampled using Dr.View/LINUX software. The ratio of the regional to cerebellar SUV (SUVR) at 40–60 min post-injection was calculated, and averaged SUVR values in the frontal, temporal, parietal and posterior cingulate cortices were considered representative of BF-227 retention in the neocortex (neocortical SUVR).

3.2. Statistical analysis

Statistical comparison of PET and MRI measurements in the four groups was performed via an analysis of variance followed by a Bonferroni multiple comparisons test with a significance level of $p<0.05$. Statistical comparisons of age and MMSE scores in the four groups were performed using a Kruskal–Wallis test followed by a Dunn's multiple comparison test with a significance level of $p<0.05$. Correlations between the MMSE score and BF-227 retention in the neocortex or the cerebral atrophy index were examined using a non-parametric Spearman's rank correlation analysis. Correlations between the brain atrophy index and BF-227 retention were determined using Pearson's correlations. A linear model was applied to the data to obtain a correlation coefficient and *p* value. These analyses were performed using GraphPad Prism5 software (GraphPad, San Diego, CA).

4. Results

In order to confirm the selective binding ability of BF-227 to Aβ deposits, neuropathological examination was initially performed using BF-227 staining of AD temporal brain sections. Senile plaques were selectively stained with BF-227 and the staining pattern coincided well with Aβ immunostaining in an adjacent section (Fig. 1). Strikingly, cored plaques were intensely stained with BF-227, indicating preferential BF-227 binding to dense Aβ fibrils. Next,

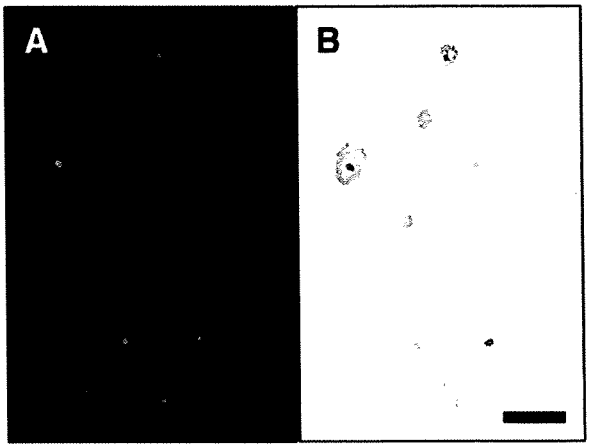

Fig. 1. (A) Neuropathological staining of human brain sections by BF-227. Amyloid plaques are clearly stained with BF-227 in AD temporal brain sections (B) BF-227 staining correlates well with Aβ immunostaining in adjacent sections. Scale bar = 100 μm.

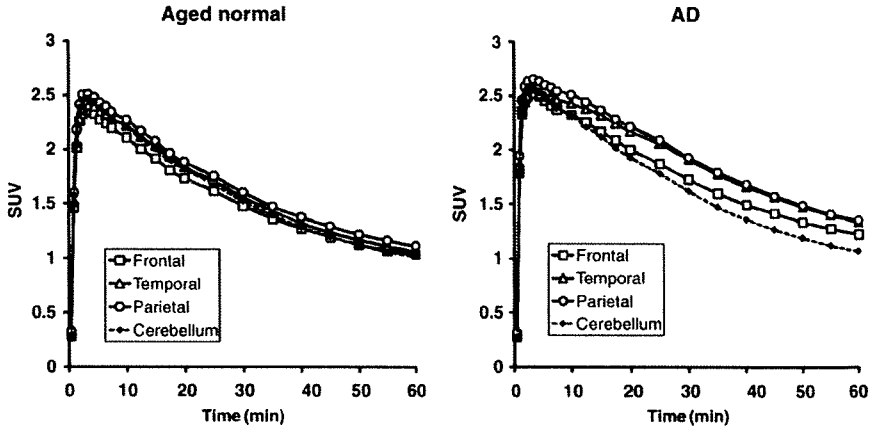

Fig. 2. Tissue time activity data for [^{11}C]BF-227–PET. SUV time activity curves of [^{11}C]BF-227 in the frontal cortex, lateral temporal cortex, parietal cortex and cerebellum are shown. Each point represents the mean of 12 control subjects (left) and 15 AD patients (right).

we performed clinical PET using [^{11}C]BF-227 in AD patients, MCI subjects and control subjects. The tissue time activity curves from [^{11}C]BF-227–PET in 15 AD patients and 12 normal controls are shown in Fig. 2. In AD patients, the frontal, temporal and parietal cortices retained [^{11}C]BF-227 to a greater extent at later time points, compared with controls. AD patients showed significantly higher SUVs in the temporal cortex and average neocortex than controls, but not in the cerebellum (Table 2). Therefore, neocortical SUV elevation in AD patients presumably reflects the specific binding of BF-227 to amyloid plaques. Representative images of [^{11}C]BF-227–PET and T1-weighted MRI in a normal control (70-year-old female, MMSE score 29), a MCI non-converter (76-year-old male, MMSE score 27), a MCI converter (85-year-old male, MMSE score 23), and an AD patient (62-year-old female, MMSE score 20) are shown in Fig. 3. Increased BF-227 retention was evident in both the MCI converter and the AD patient, but not in the control subject or the MCI non-converter. In AD patients, BF-227 SUVRs in the frontal, temporal, parietal and posterior cingulate cortices were significantly higher compared to the control subjects and the MCI non-converters (Table 2). A significant elevation of BF-227 SUVR was additionally observed in the frontal, temporal and parietal cortices of MCI converters compared with the control subjects. Consequently, the average neocortical SUVR was significantly higher in the AD patients and MCI converters than in normal subjects and MCI non-converters (Table 2). When a neocortical BF-227 SUVR of 1.11 (1.5SD above control mean) was used as a cut-off, sensitivity of 100% and a specificity of 91.7% in the discrimination between AD patients and normal subjects were achieved.

The voxel-based comparison of gray matter images using SPM5 demonstrated a significant decline of gray matter concentrations in the left ($-28, 14, -26, x, y, z; Z=5.26$) and the right ($32, 18, -26, x, y, z; Z=5.24$) medial temporal cortices of AD patients, compared with control subjects (Fig. 4A). SPM2 analysis using the same samples also showed a reduction of gray matter concentrations in nearly the same region and significance (data not shown). We drew the ROI in the parahippocampal area (Fig. 4B) and performed a comparison between the four groups. Significantly lower gray matter intensity was observed in the AD patients, MCI converters and MCI non-converters than in controls (Table 2, Fig. 5). However, age-related changes may be a confounding factor resulting in lower gray matter intensity in MCI groups, as MCI subjects were older than the normal control group. When a parahippocampal ROI value from SPM5 of 0.537 (2SD below control mean) was used as a cut-off, a sensitivity of 80.0% and a specificity of 100% were achieved in the discrimination between AD patients and normal subjects. No significant inter-group difference was observed in the percent global atrophy in VBM analysis due to substantial differences between individuals.

We focused on the comparison between the MCI converters and the non-converters, because these two populations showed no significant difference in age or MMSE scores. A significant inter-group difference was observed in the frontal and the average neocortical SUVR assayed by BF-227–PET, but not in the percent global atrophy or parahippocampal ROI value obtained by VBM–MRI (Table 2, Fig. 5). However, MCI converters showed a tendency toward lower parahippocampal ROI value derived from SPM5 than MCI non-converters.

Table 2
Summary of imaging measures.

	Normal	MCI non-converter	MCI converter	AD
BF-227 SUV in cerebellum	1.10 ± 0.19	1.08 ± 0.17	1.16 ± 0.22	1.16 ± 0.16
BF-227 SUV in frontal cortex	1.11 ± 0.19	1.10 ± 0.16	1.36 ± 0.33	1.31 ± 0.22
BF-227 SUV in temporal cortex	1.14 ± 0.19	1.19 ± 0.18	1.39 ± 0.28	1.45 ± 0.24[a]
BF-227 SUV in parietal cortex	1.20 ± 0.21	1.20 ± 0.18	1.38 ± 0.29	1.46 ± 0.23
BF-227 SUV in posterior cingulate cortex	1.22 ± 0.22	1.23 ± 0.22	1.39 ± 0.27	1.47 ± 0.21
Average neocortical BF-227 SUV	1.17 ± 0.20	1.18 ± 0.18	1.38 ± 0.29	1.42 ± 0.22[a]
BF-227 SUVR in frontal cortex	1.01 ± 0.06	1.02 ± 0.07	1.16 ± 0.10[a,b]	1.13 ± 0.08[a,b]
BF-227 SUVR in temporal cortex	1.04 ± 0.04	1.10 ± 0.07	1.20 ± 0.07[a]	1.24 ± 0.08[a,b]
BF-227 SUVR in parietal cortex	1.09 ± 0.04	1.12 ± 0.05	1.18 ± 0.07[a]	1.25 ± 0.08[a,b]
BF-227 SUVR in posterior cingulate cortex	1.11 ± 0.06	1.14 ± 0.07	1.20 ± 0.09	1.26 ± 0.05[a,b]
Average neocortical BF-227 SUVR	1.06 ± 0.04	1.09 ± 0.06	1.19 ± 0.07[a,b]	1.22 ± 0.06[a,b]
Percent global atrophy in VBM–MRI	4.24 ± 3.49	7.35 ± 5.94	5.96 ± 3.06	8.53 ± 4.44
Parahippocampal ROI value in VBM–MRI (SPM2)	0.642 ± 0.034	0.569 ± 0.039[a]	0.553 ± 0.044[a]	0.541 ± 0.055[a]
Parahippocampal ROI value in VBM–MRI (SPM5)	0.605 ± 0.034	0.510 ± 0.051[a]	0.473 ± 0.060[a]	0.475 ± 0.068[a]

[a] $p<0.05$ vs. aged normal.
[b] $p<0.05$ vs. MCI non-converter.

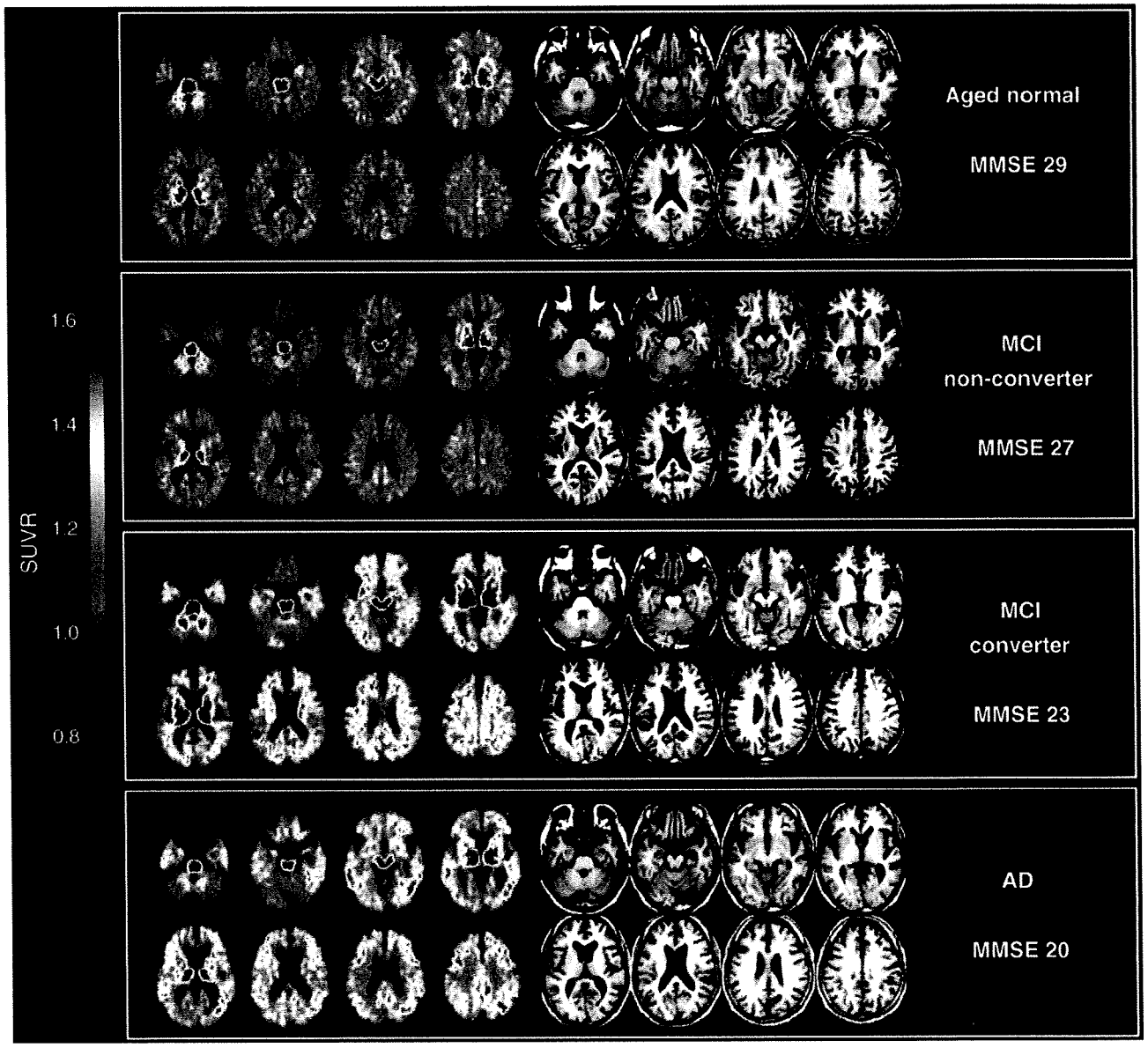

Fig. 3. Representative images of [^{11}C]BF-227–PET SUVR between 20 and 40 min post-injection (left) and T1-weighted MRI (right) in a control subject, a MCI non-converter, a MCI converter and an AD subject. The degree of [^{11}C]BF-227 retention is shown by color intensity from yellow to red in the cortex.

When we used a neocortical BF-227 SUVR of 1.11 as a cut-off, we achieved a sensitivity of 100% and a specificity of 71.4% in the discrimination between MCI converters and the MCI non-converters. These values were superior to the results of the parahippocampal ROI value derived from SPM5 (cut-off value: 0.537), which showed a sensitivity of 83.3% and a specificity of 42.9%. These data suggest that BF-227–PET is a better predictor of conversion from MCI to AD than VBM–MRI.

Next, we examined the correlations between MMSE scores and the three volume measurements (Fig. 6). When all subjects ($N=40$) were included in this analysis, a significant negative correlation was observed in all three measurements (BF-227 SUVR $r=-0.740$, $p<0.001$; percent global atrophy $r=-0.491$, $p=0.001$; parahippocampal ROI from SPM2 $r=0.674$, $p<0.001$; and parahippocampal ROI from SPM5 $r=0.687$, $p<0.001$). However, when we confined the analysis to the combined group of AD patients and MCI converters, we observed a significant correlation only between the percent global atrophy and the MMSE score (Spearman $r=-0.459$, $p=0.036$). In contrast, no significant correlation was observed between the parahippocampal ROI from SPM2 and the MMSE (Spearman $r=0.192$), between the parahippocampal ROI from SPM5 and the MMSE (Spearman $r=0.181$) or between the BF-227 SUVR in the neocortex and the MMSE (Spearman $r=-0.200$). Finally, no significant correlation was observed between the BF-227 SUVR and the percent global atrophy or parahippocampal atrophy in the analysis of all subjects.

5. Discussion

In the present study, MCI converters were more clearly distinguished from MCI non-converters by BF-227–PET than by VBM–MRI. The MCI non-converters showed a normal distribution of BF-227 except for one case, but also showed lower gray matter density in the parahippocampal gyrus than did normal controls. As a result, BF-227–PET achieved higher sensitivity and specificity in the discrimination between MCI converters and MCI non-converters than did VBM–MRI.

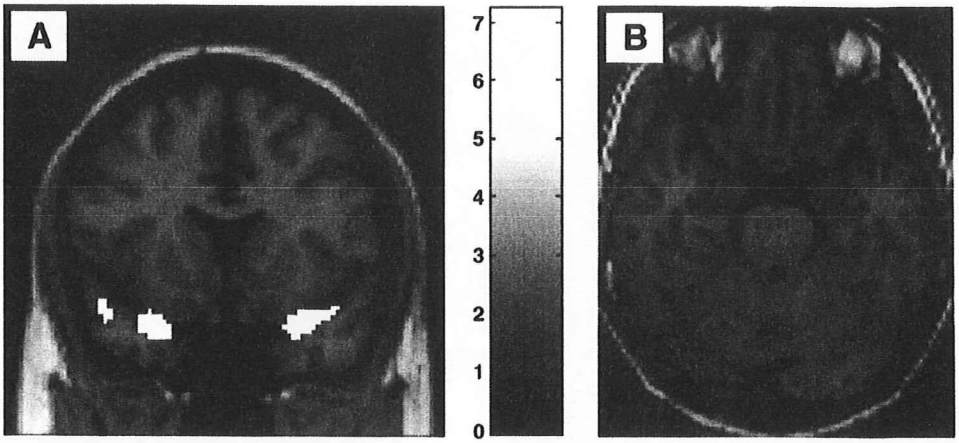

Fig. 4. (A) Areas of reduction in gray matter density of AD patients compared with aged normal controls. $p<0.05$, corrected for multiple comparisons. Left in the image is left in the brain. Color bars represent T values. (B) Regions of interest within the parahippocampal gyrus.

Our results strongly suggest that amyloid imaging using BF-227–PET will be a useful tool to predict conversion from MCI to AD, as previously shown for PIB–PET. [17,18] However, cerebral gray matter loss as determined by VBM–MRI was better correlated with the clinical severity of AD than BF-227–PET. Used together, BF-227–PET and VBM–MRI could be an effective method for the early diagnosis and severity tracking of AD. Our findings may be compatible with the theory that amyloid deposition reaches equilibrium or plateaus at an early stage of AD, making in vivo amyloid imaging useful in the examination of pre-symptomatic subjects [15,16]. Aβ deposition is a pathological hallmark of AD, but may also occur in normal elderly individuals who do not exhibit apparent cognitive decline. In fact, a PIB–PET study showed that 22% of healthy elderly individuals showed increased cortical PIB binding, indicating the presence of Aβ plaques in these non-symptomatic subjects [15]. A strong relationship between the impairment of episodic memory and PIB binding has also been shown both in subjects with MCI and in the normal population, suggesting that individuals with increased cortical PIB

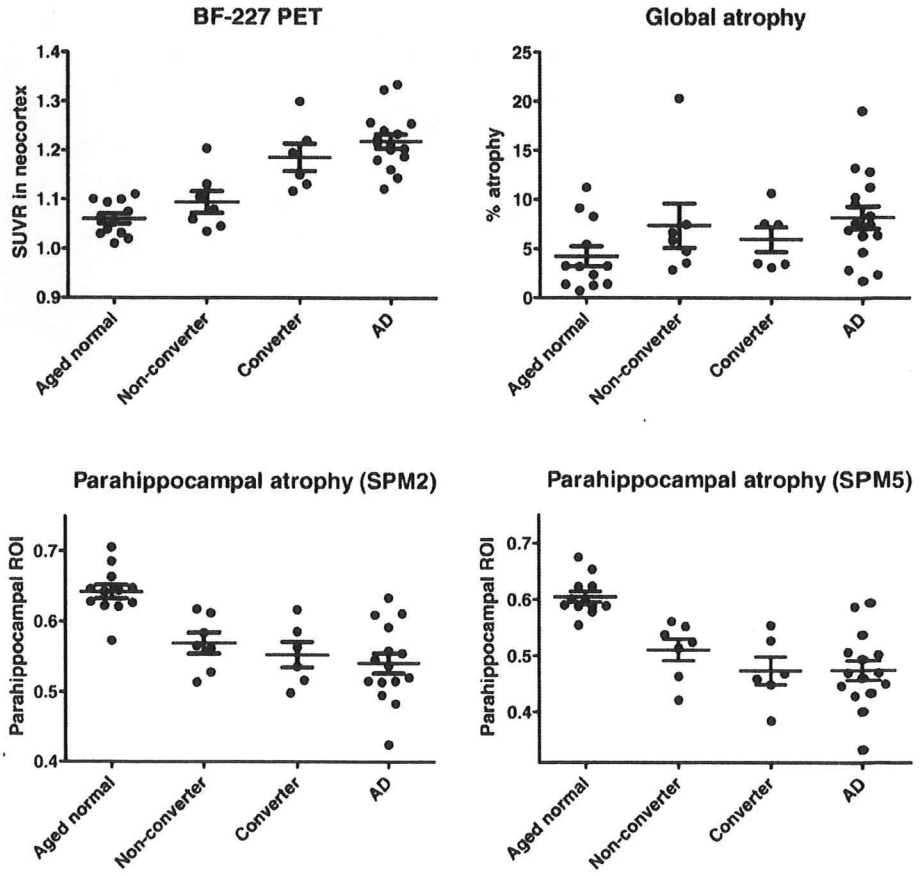

Fig. 5. Comparison of BF-227 SUVR in the neocortex (upper left), the percent global atrophy (upper right), the parahippocampal region of interest (ROI) value from gray matter images processed by SPM2 (lower left) and the parahippocampal ROI value from gray matter images processed by SPM5 (lower right) in control subjects, MCI non-converters, converters and AD patients.

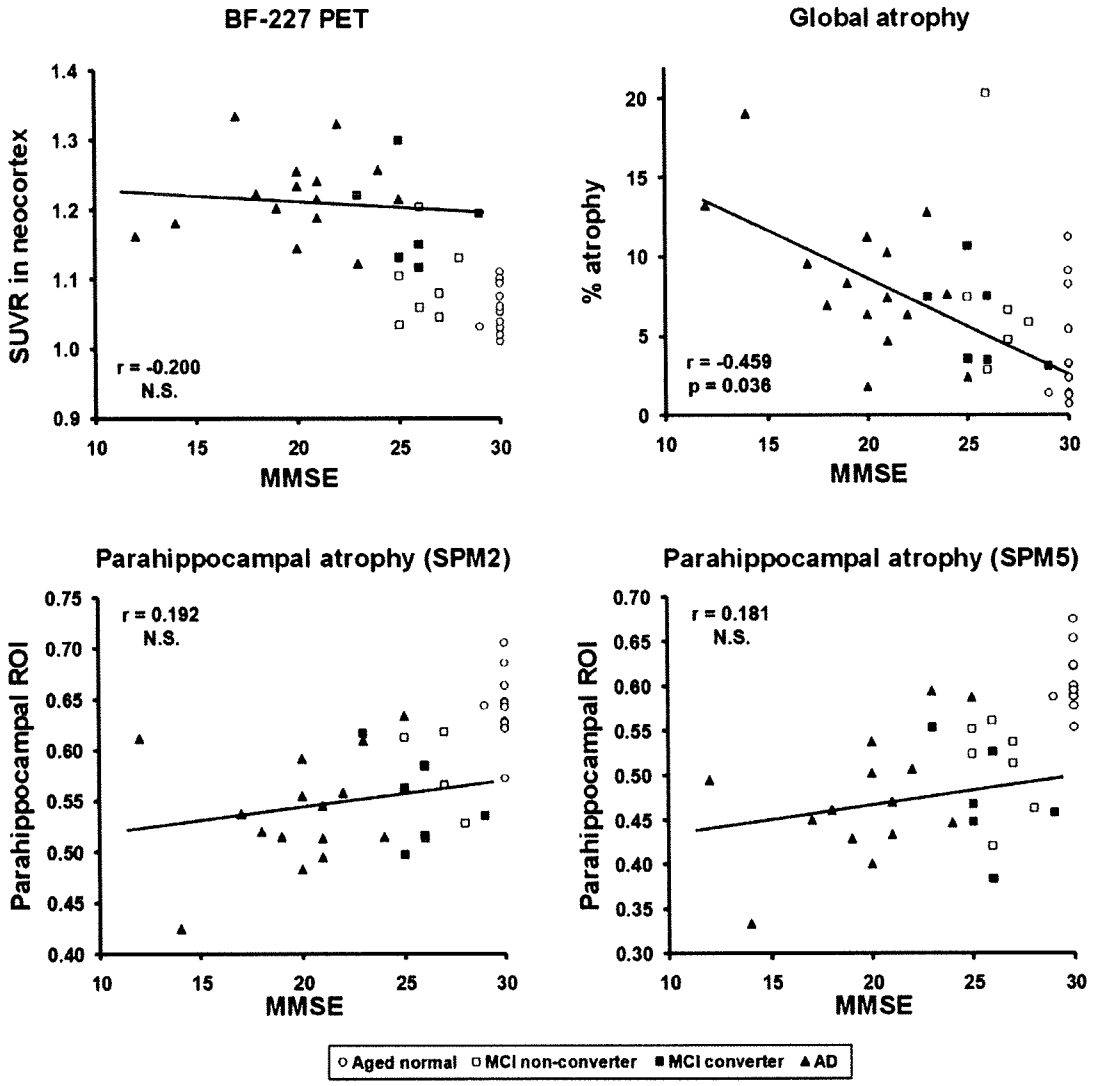

Fig. 6. The correlations of MMSE scores with the BF-227 SUVR in the neocortex (upper left), the percent global atrophy (upper right), the parahippocampal region of interest (ROI) value from gray matter images processed by SPM2 (lower left), and the parahippocampal ROI value from gray matter images processed by SPM5 (lower right). Open circle: control; open square: MCI non-converter; filled square: MCI converter; filled triangle: AD.

binding are proceeding to AD [43]. In our study, almost all normal subjects exhibited a normal distribution of BF-227 in the brain. This finding may suggest a lower sensitivity of diffuse amyloid plaque detection by BF-227 [22]. However, the proportion of amyloid PET-positive individuals in the normal population varies greatly depending on the characteristics of the sample population. Indeed, the mean age of the control subjects in our study was somewhat younger than in previous PIB–PET studies. Therefore, a direct comparison of BF-227–PET with PIB–PET in the same normal population is necessary to compare the ability of these agents to detect early AD pathology. A longitudinal follow-up of amyloid PET-positive cases in the healthy, normal population will also elucidate whether tracer uptake reflects pre-symptomatic detection of AD or a false-positive finding. A follow-up study of the patients with AD using PIB–PET showed that the amyloid deposition remains high but stable, despite decreases in regional glucose metabolism and cognitive function.[44] Our cross-sectional analysis also revealed a plateau of cortical BF-227 uptake in early AD patients, suggesting that amyloid formation reaches a plateau early in the course of AD. A potential limitation of this study is that it used a semiquantitative SUV measure to estimate BF-227 binding to amyloid plaques. The levels of neocortical BF-227 SUV might be underestimated due to hypoperfusion in AD patients. Quantitative analysis should be performed in future analyses to eliminate the influence of blood flow change.

A previous PIB–PET study found a positive correlation between the rate of whole brain atrophy and amyloid plaque load. [45] However, a recent PET study discovered a discrepancy between regional PIB retention and gray matter loss [38]. Additionally, histopathological analysis revealed no association between Aβ burden and brain atrophy [46]. The present study also found no significant correlation between neocortical BF-227 uptake and global gray matter loss in AD patients, in agreement with these findings. In our correlation analysis of the four measurements with the MMSE scores, we confined our analysis to AD patients and MCI converters because these patients share the same pathological process underlying AD. Therefore, this is more appropriate for the correlation analysis between cognitive function and the degree of Aβ burden or cerebral atrophy induced by the pathological process of AD than an analysis using all samples, including the normal population. In this analysis, the global gray matter loss measured by VBM–MRI was better correlated with MMSE scores than was the Aβ burden measured by BF-227–PET. A similar correlation analysis performed using PIB–PET demonstrated that the

magnitudes of the correlations were greater for hippocampal atrophy than for neocortical PIB retention [38]. The current result, showing no significant correlation of the parahippocampal gray matter density with the MMSE score, seems to be inconsistent with previous PIB–PET data. We believe this discrepancy to be due mainly to differences in the sample population. The analysis in the previous PIB–PET study was performed using all the subjects, including the normal controls; our analysis was confined to AD patients and MCI converters who had already developed severe memory decline and probably substantial neuron loss in the hippocampus. These results suggest that global, rather than parahippocampal, gray matter loss is a potent indicator of dementia severity after the onset of memory loss in AD. We hope to explore the relationship between these imaging measurements and the impairment of episodic memory function in a future study.

It has been reported that the degree or rate of change of cerebral atrophy as measured by MRI analysis is closely related to the clinical progression of dementia [29,30]. Karas et al. performed a VBM–MRI analysis to examine the global and regional gray matter loss in normal, MCI and AD subjects, finding a significantly lower global gray matter volume in the AD subjects and an intermediate volume in the MCI subjects [31]. They followed the MCI subjects and observed greater gray matter loss in the MCI converters than in non-converters [37]. Another study also revealed different patterns of gray matter density distribution between MCI converters and non-converters [35]. From these findings, it appears that gray matter loss in VBM is a good indicator of conversion from MCI to AD. We failed to demonstrate significant inter-group differences between the MCI converters and non-converters, although the MCI converters showed a tendency toward lower parahippocampal gray matter density than did the non-converters. This, however, may be due to the small sample size and insufficient follow-up period (over two years) of the MCI subjects in this study. For example, one MCI non-converter in our study showed an abnormality in both the BF-227 SUVR and parahippocampal gray matter density; extending the follow-up period of the MCI subjects would likely result in more consistent correlation between MCI conversion to AD and the described measurements. Additional longitudinal studies are also needed to confirm the findings we have obtained and to examine the time course of AD, including changes in the pre-symptomatic subjects, and to determine the relationship between amyloid deposition and brain atrophy as underlying factors in the pathogenesis of AD.

Acknowledgements

We appreciate the technical assistance of Dr. S. Watanuki, Dr. Y. Ishikawa, Dr. M. Mori, and Dr. K. Sugi in the clinical PET studies and the support of Fukushimura Hospital for the histochemical studies. We also thank to Dr. H. Akatsu and Dr. T. Yamamoto for supplying brain samples. This study was supported by the Program for the Promotion of Fundamental Studies in Health Science of the National Institute of Biomedical Innovation, the Industrial Technology Research Grant Program in 2004 of the New Energy and Industrial Technology Development Organization (NEDO) of Japan, Health and Labor Sciences Research Grants for Translational Research from the Ministry of Health, an Asan Trazeneca Research Grant, and the Novartis Foundation for Gerontological Research.

References

[1] Blennow K, de Leon MJ, Zetterberg H. Alzheimer's disease. Lancet 2006;368: 387–403.
[2] Drachman DA. Aging of the brain, entropy, and Alzheimer disease. Neurology 2006;67:1340–52.
[3] Braak H, Braak E. Neuropathological stageing of Alzheimer-related changes. Acta Neuropathol 1991;82:239–59.
[4] Arnold SE, Hyman BT, Flory J, Damasio AR, Van Hoesen GW. The topographical and neuroanatomical distribution of neurofibrillary tangles and neuritic plaques in the cerebral cortex of patients with Alzheimer's disease. Cereb Cortex 1991;1:103–16.
[5] Mouton PR, Martin LJ, Calhoun ME, Dal Forno G, Price DL. Cognitive decline strongly correlates with cortical atrophy in Alzheimer's dementia. Neurobiol Aging 1998;19:371–7.
[6] Masters CL, Cappai R, Barnham KJ, Villemagne VL. Molecular mechanisms for Alzheimer's disease: implications for neuroimaging and therapeutics. J Neurochem 2006;97:1700–25.
[7] Nordberg A. PET imaging of amyloid in Alzheimer's disease. Lancet Neurol 2004;3: 519–27.
[8] Villemagne VL, Rowe CC, Macfarlane S, Novakovic KE, Masters CL. Imaginem oblivionis: the prospects of neuroimaging for early detection of Alzheimer's disease. J Clin Neurosci 2005;12:221–30.
[9] Mathis CA, Klunk WE, Price JC, DeKosky ST. Imaging technology for neurodegenerative diseases: progress toward detection of specific pathologies. Arch Neurol 2005;62:196–200.
[10] Nordberg A. Amyloid imaging in Alzheimer's disease. Curr Opin Neurol 2007;20: 398–402.
[11] Small GW, Kepe V, Ercoli LM, Siddarth P, Bookheimer SY, Miller KJ, et al. PET of brain amyloid and tau in mild cognitive impairment. N Engl J Med 2006;355:2652–63.
[12] Klunk WE, Engler H, Nordberg A, Wang Y, Blomqvist G, Holt DP, et al. Imaging brain amyloid in Alzheimer's disease with Pittsburgh Compound-B. Ann Neurol 2004;55:306–19.
[13] Price JC, Klunk WE, Lopresti BJ, Lu X, Hoge JA, Ziolko SK, et al. Kinetic modeling of amyloid binding in humans using PET imaging and Pittsburgh Compound-B. J Cereb Blood Flow Metab 2005;25:1528–47.
[14] Lopresti BJ, Klunk WE, Mathis CA, Hoge JA, Ziolko SK, Lu X, et al. Simplified quantification of Pittsburgh Compound B amyloid imaging PET studies: a comparative analysis. J Nucl Med 2005;46:1959–72.
[15] Rowe CC, Ng S, Ackermann U, Gong SJ, Pike K, Savage G, et al. Imaging beta-amyloid burden in aging and dementia. Neurology 2007;68:1718–25.
[16] Mintun MA, Larossa GN, Sheline YI, Dence CS, Lee SY, Mach RH, et al. [^{11}C]PIB in a nondemented population: potential antecedent marker of Alzheimer disease. Neurology 2006;67:446–52.
[17] Fripp J, Bourgeat P, Acosta O, Raniga P, Modat M, Pike KE, et al. Appearance modeling of ^{11}C PiB PET images: characterizing amyloid deposition in Alzheimer's disease, mild cognitive impairment and healthy aging. Neuroimage 2008;43:430–9.
[18] Forsberg A, Engler H, Almkvist O, Blomquist G, Hagman G, Wall A, et al. PET imaging of amyloid deposition in patients with mild cognitive impairment. Neurobiol Aging 2008;29:1456–65.
[19] Okamura N, Suemoto T, Shimadzu H, Suzuki M, Shiomitsu T, Akatsu H, et al. Styrylbenzoxazole derivatives for in vivo imaging of amyloid plaques in the brain. J Neurosci, 2004;24:2535–41.
[20] Okamura N, Furumoto S, Funaki Y, Suemoto T, Kato M, Ishikawa Y, et al. Binding and safety profile of novel benzoxazole derivative for in vivo imaging of amyloid deposits in Alzheimer's disease. Geriatr Gerontol Int 2007;7:393–400.
[21] Furumoto S, Okamura N, Iwata R, Yanai K, Arai H, Kudo Y. Recent advances in the development of amyloid imaging agents. Curr Top Med Chem 2007;7:1773–89.
[22] Kudo Y, Okamura N, Furumoto S, Tashiro M, Furukawa K, Maruyama M, et al. 2-(2-[2-Dimethylaminothiazol-5-yl]Ethenyl)-6-(2-[Fluoro]Ethoxy)Benzoxazole: A novel PET agent for in vivo detection of dense amyloid plaques in Alzheimer's disease patients. J Nucl Med 2007;48:553–61.
[23] Fodero-Tavoletti MT, Mulligan RS, Okamura N, Furumoto S, Rowe CC, Kudo Y, et al. In vitro characterization of BF227 binding to α-synuclein/Lewy Bodies. Eur J Pharmacol 2009;617:54–8.
[24] Ishii K, Hashimoto M, Kimura Y, Sakata M, Oda K, Kawasaki K, et al. Direct comparison of in vivo accumulation of ^{11}C-PIB and ^{11}C-BF227 in Alzheimer's disease. Alzheimer's and Dementia, vol. 4, Issue 4; July 2008. p. T49. Supplement 1.
[25] Tiraboschi P, Hansen LA, Thal LJ, Corey-Bloom J. The importance of neuritic plaques and tangles to the development and evolution of AD. Neurology 2004;62:1984–9.
[26] Price JL, Morris JC. Tangles and plaques in nondemented aging and "preclinical" Alzheimer's disease. Ann Neurol 1999;45:358–68.
[27] Morris JC, Storandt M, Miller JP, McKeel DW, Price JL, Rubin EH, et al. Mild cognitive impairment represents early-stage Alzheimer disease. Arch Neurol 2001;58:397–405.
[28] Wang J, Dickson DW, Trojanowski JQ, Lee VM. The levels of soluble versus insoluble brain Abeta distinguish Alzheimer's disease from normal and pathologic aging. Exp Neurol 1999;158:328–37.
[29] Fox NC, Crum WR, Scahill RI, Stevens JM, Janssen JC, Rossor MN. Imaging of onset and progression of Alzheimer's disease with voxel-compression mapping of serial magnetic resonance images. Lancet 2001;358:201–5.
[30] Jack Jr CR, Shiung MM, Gunter JL, O'Brien PC, Weigand SD, Knopman DS, et al. Comparison of different MRI brain atrophy rate measures with clinical disease progression in AD. Neurology 2004;62:591–600.
[31] Karas GB, Scheltens P, Rombouts SA, Visser PJ, van Schijndel RA, Fox NC, et al. Global and local gray matter loss in mild cognitive impairment and Alzheimer's disease. Neuroimage 2004;23:708–16.
[32] Killiany RJ, Gomez-Isla T, Moss M, Kikinis R, Sandor T, Jolesz F, et al. Use of structural magnetic resonance imaging to predict who will get Alzheimer's disease. Ann Neurol 2000;47:430–9.
[33] Bell-McGinty S, Lopez OL, Meltzer CC, Scanlon JM, Whyte EM, Dekosky ST, et al. Differential cortical atrophy in subgroups of mild cognitive impairment. Arch Neurol 2005;62:1393–7.
[34] Chetelat G, Landeau B, Eustache F, Mezenge F, Viader F, de la Sayette V, et al. Using voxel-based morphometry to map the structural changes associated with rapid conversion in MCI: a longitudinal MRI study. Neuroimage 2005;27:934–46.
[35] Bozzali M, Filippi M, Magnani G, Cercignani M, Franceschi M, Schiatti E, et al. The contribution of voxel-based morphometry in staging patients with mild cognitive impairment. Neurology 2006;67:453–60.

[36] Hämäläinen A, Tervo S, Grau-Olivares M, Niskanen E, Pennanen C, Huuskonen J, et al. Voxel-based morphometry to detect brain atrophy in progressive mild cognitive impairment. Neuroimage 2007;37:1122–31.
[37] Karas G, Sluimer J, Goekoop R, van der Flier W, Rombouts SA, Vrenken H, et al. Amnestic mild cognitive impairment: structural MR imaging findings predictive of conversion to Alzheimer disease. Am J Neuroradiol 2008;29:944–9.
[38] Jack Jr CR, Lowe VJ, Senjem ML, Weigand SD, Kemp BJ, Shiung MM, et al. ^{11}C PiB and structural MRI provide complementary information in imaging of Alzheimer's disease and amnestic mild cognitive impairment. Brain 2008;131:665–80.
[39] McKhann G, Drachman D, Folstein M, Katzman R, Price D, Stadlan EM. Clinical diagnosis of Alzheimer's disease: report of the NINCDS-ADRDA Work Group under the auspices of Department of Health and Human Services Task Force on Alzheimer's Disease. Neurology 1984;34:939–44.
[40] Petersen RC, Smith GE, Waring SC, Ivnik RJ, Tangalos EG, Kokmen E. Mild cognitive impairment: clinical characterization and outcome. Arch Neurol 1999;56:303–8.
[41] Ashburner J, Friston KJ. Voxel-based morphometry—the methods. Neuroimage 2000;11:805–21.
[42] Hirata Y, Matsuda H, Nemoto K, Ohnishi T, Hirao K, Yamashita F, et al. Voxel-based morphometry to discriminate early Alzheimer's disease from controls. Neurosci Lett 2005;382:269–74.
[43] Pike KE, Savage G, Villemagne VL, Ng S, Moss SA, Maruff P, et al. Beta-amyloid imaging and memory in non-demented individuals: evidence for preclinical Alzheimer's disease. Brain 2007;130:2837–44.
[44] Engler H, Forsberg A, Almkvist O, Blomquist G, Larsson E, Savitcheva I, et al. Two-year follow-up of amyloid deposition in patients with Alzheimer's disease. Brain 2006;129:2856–66.
[45] Archer HA, Edison P, Brooks DJ, Barnes J, Frost C, Yeatman T, et al. Amyloid load and cerebral atrophy in Alzheimer's disease: an ^{11}C-PIB positron emission tomography study. Ann Neurol 2006;60:145–7.
[46] Josephs KA, Whitwell JL, Ahmed Z, Shiung MM, Weigand SD, Knopman DS, et al. Beta-amyloid burden is not associated with rates of brain atrophy. Ann Neurol 2008;63:204–12.

European Journal of Pharmacology 617 (2009) 54–58

Contents lists available at ScienceDirect

European Journal of Pharmacology

journal homepage: www.elsevier.com/locate/ejphar

Neuropharmacology and Analgesia

In vitro characterisation of BF227 binding to α-synuclein/Lewy bodies

Michelle T. Fodero-Tavoletti [a,b,c], Rachel S. Mulligan [f], Nobuyuki Okamura [e], Shozo Furumoto [d], Christopher C. Rowe [f], Yukitsuka Kudo [d], Colin L. Masters [c], Roberto Cappai [a,b,c], Kazuhiko Yanai [e], Victor L. Villemagne [a,c,f,*]

[a] Department of Pathology, The University of Melbourne, VIC, Australia
[b] Bio21 Molecular and Biotechnology Institute, The University of Melbourne, VIC, Australia
[c] The Mental Health Research Institute of Victoria, Tohoku University, Sendai, Japan
[d] Biomedical Engineering Research Organization, Tohoku University, Sendai, Japan
[e] Department of Pharmacology, Tohoku University, Sendai, Japan
[f] Department of Nuclear Medicine, Austin Health, Centre for PET, VIC, Australia

ARTICLE INFO

Article history:
Received 4 March 2009
Received in revised form 6 June 2009
Accepted 22 June 2009
Available online 1 July 2009

Keywords:
BF227
α-synuclein
Positron emission tomography
Dementia with Lewy bodies
Aβ (amyloid-β)
Imaging

ABSTRACT

Amyloid-β (Aβ) plaques are a pathological hallmark of Alzheimer's disease and a current target for positron emission tomography (PET) imaging agents. Whilst [^{11}C]-PiB is currently the most widely used PET ligand in clinic, a novel family of benzoxazole compounds have shown promise as Aβ imaging agents; particularly BF227. We characterised the in vitro binding of [^{18}F]-BF227 toward α-synuclein to address its selectivity for Aβ pathology, to establish whether [^{18}F]-BF227 binds to α-synuclein/Lewy bodies, in addition to Aβ plaques. In vitro [^{18}F]-BF227 saturation studies were conducted with 200 nM α-synuclein or $A\beta_{1-42}$ fibrils or 100 μg of Alzheimer's disease, pure dementia with Lewy bodies or control brain homogenates. Non-specific binding was established with PiB (1 μM). In vitro binding studies indicated that [^{18}F]-BF227 binds with high affinity to two binding sites on $A\beta_{1-42}$ fibrils (K_{D1} = 1.31 and K_{D2} = 80 nM, respectively) and to one class of binding sites on α-synuclein fibrils (K_D = 9.63nM). [^{18}F]-BF227 bound to Aβ-containing Alzheimer's disease brain (K_D = 25 ± 0.5 nM), but failed to bind to Aβ-free dementia with Lewy bodies or age-matched control homogenates. Moreover, BF227 labelled both Aβ plaques and Lewy bodies in immunohistochemical/fluorescence analysis of human Alzheimer's disease and Parkinson's disease brain sections, respectively. This study suggests that [^{18}F]-BF227 is not Aβ-selective. Evaluation of BF227 as a potential biomarker for Parkinson's disease is warranted.

1. Introduction

Currently, there is no cure for Alzheimer's disease, an age-related neurodegenerative disease, clinically characterised by dementia. The Alzheimer's disease brain is pathologically characterised by the presence of (i) extracellular amyloid plaques comprising amyloid-β (Aβ); (ii) intracellular neurofibrillary tangles composed of hyperphosphorylated tau; (iii) synaptic loss and reactive gliosis; (iv) increased oxidative damage to lipids, proteins and nucleic acids and (v) biometal dyshomeostasis (Goedert and Spillantini, 2006).

Definitive diagnosis of Alzheimer's disease and related dementias still relies upon postmortem examination. As new therapeutic strategies undergo clinical evaluation, considerable effort is now focused on biomarkers for the early and accurate diagnosis of Alzheimer's disease, as well as therapeutic monitoring. Modern molecular imaging procedures such as positron emission tomography (PET), may provide new insight into Alzheimer's disease by non-invasively identifying the underlying pathology of these diseases in the living. Of late, Pittsburgh compound B [PiB] has proven to be a successful biomarker for the in vivo quantitation of Aβ burden (Klunk et al., 2004; Rowe et al., 2007). Nonetheless, its widespread clinical use is impracticable due to the 20-minute decay half-life of carbon-11, limiting its use to centres with an on-site cyclotron. [^{18}F]-FDDNP also highlights Aβ deposits in the human brain; however, FDDNP also binds to neurofibrillary tangles (Agdeppa et al., 2001), as well as PrP^{sc} (Boxer et al., 2007; Bresjanac et al., 2003). Whilst labelling with a longer half-life isotope [^{18}F] proves to be advantageous, FDDNP's lack of selectivity considerably reduces its ability to provide differential diagnosis of neurodegenerative diseases. Hence, the development of a specific

* Corresponding author. Department of Nuclear Medicine, Austin Health, Centre for PET 145 Studley Rd Heidelberg, VIC, 3084 Australia. Tel.: +61 3 9496 3321; fax: +61 3 9458 5023.
E-mail address: villemagne@petnm.unimelb.edu.au (V.L. Villemagne).

0014-2999/$ – see front matter © 2009 Elsevier B.V. All rights reserved.
doi:10.1016/j.ejphar.2009.06.042

and selective [^{18}F]-labelled imaging agent(s) for molecular Aβ imaging is highly desirable to improve diagnostic accuracy and accelerate discovery and monitoring of therapeutics.

Recently, a novel series of benzoxazole compounds have been developed as PET imaging agents; namely BF227 [2-[2-(2-dimethylaminothiazol-5-yl)ethenyl]-6-[2-(fluoro)ethoxy] benzoxazole] has been demonstrated to bind to $A\beta_{1-42}$ fibrils (with low nanomolar affinity) and Aβ plaques in Alzheimer's disease brain sections (Kudo et al., 2007). [^{11}C]-BF227-PET demonstrated retention in cerebral cortices of Alzheimer's disease patients with very little retention in normal patients; suggesting BF227 as a promising PET imaging agent for the in vivo detection of Aβ pathology in Alzheimer's disease patients. Whilst the specificity of BF227 binding to Aβ has been established, there is limited knowledge regarding its selectivity; particularly since Alzheimer's disease has been described as a 'triple brain amyloidosis' (Trojanowski, 2002), comprising Aβ, tau and α-synuclein that when misfolded, comprise the principal components of senile plaques, neurofibrillary tangles and Lewy bodies. Furthermore, the majority of dementia with Lewy bodies cases exhibit extensive cortical Aβ deposition along the pathognomonic Lewy bodies (McKeith et al., 2005). Hence, critical assessment of new radiotracers such as BF227 is warranted to avoid misinterpretation of results and/or incorrect diagnosis. Whilst BF227 binding to neurofibrillary tangles has previously been examined (Kudo et al., 2007), the potential of BF227 binding to α-synuclein has not been assessed. The aim of this study was to test the ability of BF227 to bind/recognise α-synuclein fibrils/Lewy bodies to establish whether [^{18}F]-BF227 is selective for Aβ pathology.

2. Materials and methods

2.1. Materials

All reagents were purchased from Sigma (St. Louis, MO), unless otherwise stated. Human $A\beta_{1-42}$ was purchased from the W. M. Keck Laboratory (Yale University, New Haven, CT).

2.1.1. Tissue collection and characterisation

Brain tissue was collected at autopsy. The sourcing and preparation of the human brain tissue were conducted by the National Neural Tissue Resource Centre. Alzheimer's disease pathological diagnosis was made according to standard NIA-Reagan Institute criteria (1997). Dementia with Lewy bodies cases was diagnosed using consensus guidelines (McKeith et al., 1996) and classified as either dementia with Lewy bodies-Aβ, being subjects with evidence of neuritic plaques and/or cerebral vascular amyloid, as determined by IHC and ELISA, or pure dementia with Lewy bodies (no significant evidence of neuritic plaques and/or cerebral vascular amyloid). Parkinson's disease pathological diagnosis was made following previously described criteria (Braak et al., 2003; Forno, 1996). Determination of age-matched controls cases were also subject to the above criteria. The number of subject cases utilised is indicated in the figure/table texts. Overall, three Alzheimer's disease, three dementia with Lewy bodies-Aβ, one pure Dementia with Lewy bodies, two Parkinson's disease and three age-matched control subjects were utilised in this study.

2.1.2. [^{18}F] labelling of BF227

Unlabelled BF227 and 2-[2-(2-dimethylaminothiazol-5-yl)ethenyl]-6-[2-(tosyloxy)ethoxy] benzoxazole (BF-226; the precursor for [^{18}F]-BF-227) were custom synthesised by Tanabe R&D Service Co. and confirmed for purity by reverse phase high performance liquid chromatography, one dimensional NMR and mass spectrometry. [^{18}F]-BF227 was synthesised by nucleophilic substitution of the tosylate precursor (BF-226) (see below). Following a 10 min reaction at 110°C the crude reaction was partially purified on an activated Sep Pak tC18 cartridge before undergoing semi preparative reverse phase HPLC purification. Standard tC18 Sep-Pak reformulation produced [^{18}F]-BF227 in >95% radiochemical purity. The radiochemical yield was 17% (non decay corrected) and at the end of the synthesis the average specific activity was 1471 mCi/μmol/42 GBq/μmol.

Schematic for the radiosynthesis of [^{18}F]-BF227.

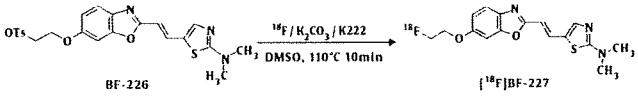

2.1.3. Preparation of amyloid fibrils

Synthetic $A\beta_{1-42}$ was dissolved in 1× PBS pH 7.7 to a final concentration of 200 μM. Recombinant human α-synuclein was expressed and purified as previously described (Cappai et al., 2005) and dissolved in 10 mM phosphate buffer pH 7.4, to a final concentration of 200 μM. These solutions were incubated at 37°C for either 2 days for $A\beta_{1-42}$ or 7 days for α-synuclein, with agitation (220 rpm, Orbital mixer incubator, Ratek). After aggregation, approximately 5% of the protein remained in the supernatant after centrifugation at 12,000×g for 20 minutes. Fibril aggregation was confirmed through ThT fluorescence spectroscopy and electron microscopy.

2.1.4. Preparation of human brain tissue for in vitro binding studies

Grey matter was isolated from the postmortem frontal cortex tissue from the Alzheimer's disease, dementia with Lewy bodies-Aβ, pure dementia with Lewy bodies and age-matched control subjects. Isolated tissue was then homogenised in 1× PBS (without calcium and magnesium), utilising an ultrasonic cell disrupter (2 × 30 s, 24,000 rpm; Virsonic 600, Virtis). Protein concentration was determined using the BCA protein assay (Pierce) and brain tissue homogenates were aliquoted and frozen at −80 °C until used.

2.1.5. In vitro BF227 binding assays

Synthetic $A\beta_{1-42}$ or α-synuclein fibrils (200 nM) were incubated with increasing concentrations of [^{18}F]-BF227 (0.5–200 nM). To account for non-specific binding of [^{18}F]-BF227, the above mentioned reactions were duplicated in the presence of unlabelled 1 μM PiB. The binding reactions were incubated for 1 h at room temperature in 200 μl of assay buffer [PBS, minus Mg^{2+} and Ca^{2+} (JRH Biosciences, Kansas, USA); 0.1% BSA]. Binding of [^{18}F]-BF227 to human brain homogenates was assessed by incubating 100 μg brain homogenate from Alzheimer's disease, pure dementia with Lewy bodies (Aβ-free) and age-matched control subjects with increasing concentrations of [^{18}F]-BF227 (0.1–250nM [^{18}F]-BF227 in the absence or presence of unlabelled PiB (1 μM)), as described above. Bound from free radioactivity was separated by filtration under reduced pressure (MultiScreen HTS Vacuum Manifold; MultiScreen HTS 96-well filtration plates; 0.65 μm, Millipore). Filters were washed three times with 200 μl assay buffer and incubated overnight in 3 ml scintillation fluid. Washed filters were assayed for radioactivity in an automatic gamma counter (Wallac 1480 Wizard 3″; Perkin Elmer). Binding data were analysed with curve fitting software that calculates the K_D and B_{max} using nonlinear regression according to the equation:

$$Y = B_{max} \cdot X$$

$$K_D + X$$

(GraphPad Prism Version 1.0, GraphPad Software, San Diego, CA). All experiments were conducted in triplicate.

2.2. Immunohistochemistry (IHC) and Fluorescence Analysis

Brain tissue from Alzheimer's disease and Parkinson's disease subjects was fixed in 10% formalin/PBS and embedded in paraffin. For immunohistochemistry and fluorescence analysis of BF227, 7 μm serial sections were assessed. Serial sections were deparaffinized and treated with 80% formic acid for 5 min and endogenous peroxidase

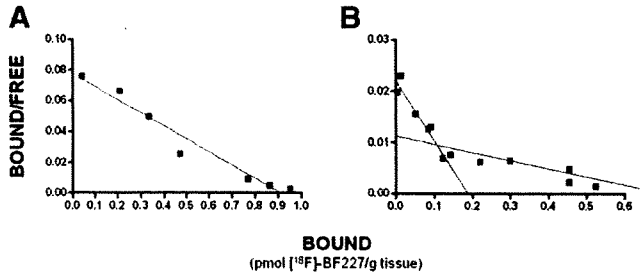

Fig. 1. In vitro binding studies indicate one class of [^{18}F]-BF227 binding sites on α-synuclein fibrils. Scatchard plots of [^{18}F]-BF227 binding to synthetic (A) α-synuclein or (B) $A\beta_{1-42}$ fibrils. (A) Scatchard analysis identified one class of BF227 binding sites on α-synuclein fibrils (K_D of 9.63 nM and B_{max} of 2.76 pmol BF227/nmol α-synuclein). (B) Scatchard analysis identified two classes of BF227 binding sites on $A\beta_{1-42}$; a high affinity binding site with K_D and B_{max} of 1.31 nM and 0.171 pmol BF227/nmol $A\beta_{1-42}$, respectively and a low affinity binding site with K_D and B_{max} of 80.0 nM and 2.96 pmol BF227/nmol $A\beta_{1-42}$, respectively. Binding data were analysed using GraphPad Software (Version 1.0, San Diego, CA). This figure is the average of at least three independent experiments.

activity was blocked utilising 3% hydrogen peroxide. Serial tissue sections were stained in the following order: the first and third sections were immunostained with 97/8 or 1e8 antibodies to identify Lewy bodies or Aβ plaques, respectively and the second section was incubated with BF227. For immunostaining, sections were treated with blocking buffer (20% fetal calf serum, 50 mM Tris–HCl, 175 mM NaCl pH 7.4) before immunostaining with primary antibodies to α-synuclein [97/8; 1:2000 dilution (Culvenor et al., 1999)] or Aβ (1e8; 1:50), for 1 h at room temperature. Visualisation of antibody reactivity was achieved using the LSAB™ kit (labelled streptavidin–biotin, DAKO) and sections were then incubated with hydrogen-peroxidase–diaminobenzidine (H_2O_2–DAB) to visualise the α-synuclein or Aβ-positive deposits. Sections were counterstained with Mayer's hematoxylin. To assess BF227 fluorescence, quenching to minimise autofluorescence was first performed on deparaffinized tissue sections by treatment with 0.25% $KMnO_4$/PBS for 20 min prior to washing (PBS) and incubation with 1% potassium metabisulfite/1% oxalic acid/PBS for 5 min. Following autofluorescence quenching, sections were blocked in 2% BSA/PBS pH 7.0 for 10 min and stained with 100 μM BF227 for 30 min. Washed (PBS) sections were then mounted in non-fluorescent mounting media (DAKO). Epifluorescence images were visualised using a Zeiss microscope (47CFP; filter set 47 (EM BP 436/20, BS FT 455, EM BP480/40). Co-localisation of the BF227 and antibody signals was assessed by overlaying images from each of the stained serial tissue sections.

3. Results

3.1. Characteristics of [^{18}F]-BF227 Binding to Recombinant α-Synuclein and $A\beta_{1-42}$ Fibrils

To investigate the selectivity of BF227, we tested the ability of [^{18}F]-BF227 to bind to synthetic α-synuclein and $A\beta_{1-42}$ fibrils; the major component of Lewy bodies and senile plaques, respectively. The successful formation of fibrils was determined by ThT fluorescence and transmission electron microscopy, prior to conducting the binding assays (data not shown).

Assessment of [^{18}F]-BF227 binding was conducted using equimolar concentrations (200 nM, ~4.0×10^{-11} mol) of either α-synuclein or $A\beta_{1-42}$ fibrils. Scatchard analysis indicated that [^{18}F]-BF227 bound to one site on α-synuclein fibrils with high affinity (K_D 9.63nM; Fig. 1A). In contrast, two classes of binding sites exist for [^{18}F]-BF227 binding to $A\beta_{1-42}$ fibrils (high affinity K_{D1} 1.31 and low affinity K_{D2} 80nM, respectively; Fig. 1B). Despite the two classes of binding sites identified for $A\beta_{1-42}$ fibrils, the total number of binding sites was similar for both α-synuclein (B_{max} 2.76 pmol [^{18}F]-BF227/nmol α-synuclein) and $A\beta_{1-42}$ (B_{max1} 0.171 and B_{max2} 2.96 pmol [^{18}F]-BF227/nmol $A\beta_{1-42}$) fibrils.

3.2. In Vitro [^{18}F]-BF227 Binding Analysis of Human Alzheimer's Disease and Dementia With Lewy Bodies Brain

In previous studies, postmortem human brain homogenates have been extensively utilised to characterise amyloid imaging agents, including PiB (Fodero-Tavoletti et al., 2007; Klunk et al., 1995; Klunk et al., 2003; Klunk et al., 2005; Mathis et al., 2003). To further assess the selectivity of BF227, we compared the in vitro binding properties of [^{18}F]-BF227 to Aβ-containing brain homogenates (Alzheimer's disease) versus Aβ-free (non-detectable levels of Aβ) homogenates (pure dementia with Lewy bodies and age-matched control). Aβ ELISA analysis was utilised to establish the presence/absence (non-detectable levels) of Aβ, prior to conducting binding studies (data not shown). [^{18}F]-BF227 bound with high affinity to Aβ-containing brain homogenates. Scatchard analysis identified one class of binding sites within Alzheimer's disease homogenates with a K_D of 33 ± 4.8 nM and a B_{max} of 9353 pmol/[^{18}F]-BF227/g tissue (Fig. 2A). In contrast, [^{18}F]-BF227 did not bind to the α-synuclein-containing Aβ-free dementia with Lewy bodies (dementia with Lewy bodies-pure; Fig. 2B) or the Aβ-and α-synuclein-free age-matched control subjects (Fig. 2C).

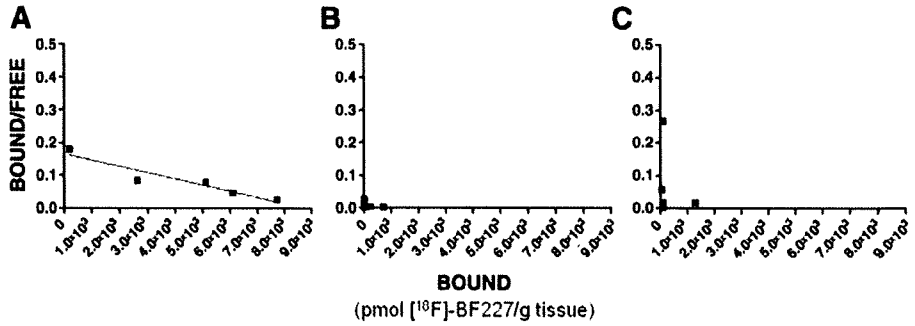

Fig. 2. In vitro binding studies demonstrate that [^{18}F]-BF227 fails to bind to pure dementia with Lewy bodies brain homogenate. Scatchard plots of [^{18}F]-BF227 binding to (A) AD, (B) age-matched control and (C) pure dementia with Lewy bodies brain homogenates. Scatchard analysis indicated that BF227 binds to Alzheimer's disease (K_D 33 ± 4.8nM, B_{max} 9353 pmol/[^{18}F]-BF227/g tissue). No significant binding of [^{18}F]-BF227/g to pure dementia with Lewy body or age-matched control subjects was observed. Binding data were analysed using GraphPad Software (Version 1.0, San Diego, CA). This figure is the average of at least three independent experiments.

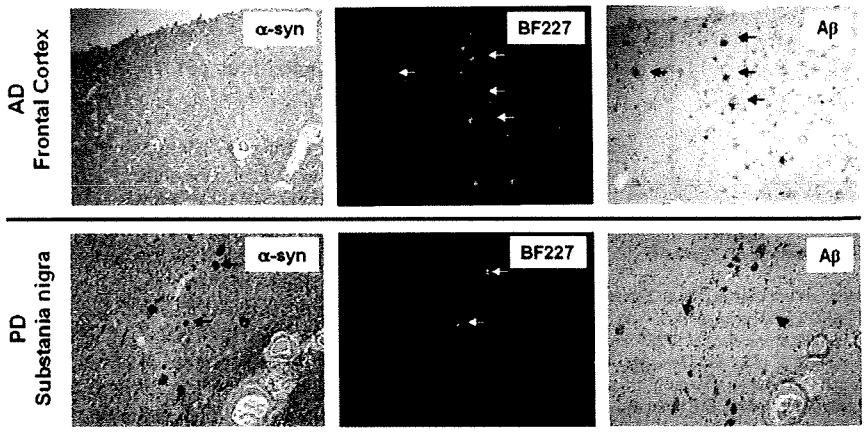

Fig. 3. Immunohistochemistry analysis indicates that BF227 binds specifically to Aβ plaques and not α-synuclein-containing Lewy bodies within the substantia nigra. Microscopy images of three serial sections (7 mm) from the frontal cortex of (A) Alzheimer's disease or (B) substantia nigra Parkinson's disease brain, immunostained with antibodies to α-synuclein (97/8; 1:2000) and Aβ (1E8; 1:50), to identify Lewy bodies and Aβ plaques respectively; or stained with 100 mM BF227. Black arrows indicate the location of Aβ plaques (top panel) and Lewy bodies (bottom panel), as determined by immunohistochemistry. White arrows indicate positive BF227 staining as detected by fluorescence, co-localising with 1E8 immunostaining of Aβ plaques in Alzheimer's disease subjects and Lewy bodies in the substantia nigra of Parkinson's disease subjects. Tissue sections were imaged using a Leica microscope and Axiocam digital camera. Scale bars, 50 mm.

3.3. BF227 and Immunohistochemical Staining of Human Alzheimer's Disease and Parkinson's Disease Subjects

As a qualitative measure of its potential binding to α-synuclein deposits/Lewy bodies by fluorescence microscopy, unlabelled BF227 was used to stain fixed serial sections from the substantia nigra of Parkinson's disease subjects. Staining of the frontal cortex of Alzheimer's disease subjects was also conducted. Parkinson's disease substantia nigra sections were chosen for their rich source of Lewy bodies. BF227 staining of the substantia nigra co-localised with immuno-reactive α-synuclein-containing Lewy bodies (Fig. 3). A comparison of the α-synuclein staining Lewy bodies with BF227 staining suggested that BF227 binds to Lewy bodies as well as Aβ stained plaques.

4. Discussion

The ongoing quest for specific and selective PET imaging agents is imperative for the early diagnosis, treatment, development and monitoring of neurodegenerative diseases, such as Alzheimer's disease. To date, the design and testing of PET imaging candidates have suggested that compounds based on histological dyes whilst specific, are not selective for Aβ pathology. Benzoxazole compounds/derivatives represent a promising new family of imaging agents that may overcome some of the limitations of current PET ligands.

In vitro binding studies indicated that [^{18}F]-BF227 bound significantly to $A\beta_{1-42}$ fibrils; exhibiting two classes of binding sites. Previous studies (Kudo et al., 2007) assessing the binding affinity of BF227 to $A\beta_{1-42}$ fibrils utilised a competition binding assay that was incapable of detecting multiple classes of binding sites. This study is the first to suggest the existence of two binding sites for benzoxazole compounds on $A\beta_{1-42}$ fibrils. Binding of [^{18}F]-BF227 to α-synuclein fibrils was observed only at an equimolar concentration to $A\beta_{1-42}$ fibrils although, with a ~10-fold lower affinity when compared to $A\beta_{1-42}$ fibrils (Fig. 1A). The lower affinity of [^{18}F]-BF227 for synthetic α-synuclein fibrils as compared to $A\beta_{1-42}$ fibrils and the concentration of [^{18}F]-BF227 (~1 nM) typically achieved during PET studies, suggests that the binding of [^{18}F]-BF227 to α-synuclein-containing Lewy bodies should not contribute significantly to the [^{18}F]-BF227-PET signal.

Despite the results obtained for synthetic $A\beta_{1-42}$ fibrils, in vitro studies in brain homogenates failed to show two binding sites. Nevertheless, a high affinity K_D value in the low nanomolar range was observed. This distinction may reflect the fact that Aβ plaques are not only composed of $A\beta_{1-42}$, but also $A\beta_{1-40}$ and other longer or truncated species of Aβ (i.e. $A\beta_{1-39}$ and $A\beta_{1-43}$) within the Alzheimer's disease brain. Despite the binding of [^{18}F]-BF227 to α-synuclein fibrils, no binding of [^{18}F]-BF227 was detected in pure dementia with Lewy bodies homogenates, devoid of Aβ plaques. This observation may indicate that the density of α-synuclein-containing Lewy bodies present in the pure dementia with Lewy bodies homogenates analysed may be low and therefore undetectable by [^{18}F]-BF227. Our previous studies assessing PiB binding to α-synuclein fibrils and pure dementia with Lewy bodies brain homogenates yielded similar results and as remarked there, the concentration of α-synuclein fibrils utilised for the in vitro studies may be physiologically unattainable, explaining the discrepancy between fibril and dementia with Lewy bodies brain homogenate results (Fodero-Tavoletti et al., 2007).

Consistent with previous reports, BF227 staining of Aβ plaques was clearly evident in the Alzheimer's disease brain sections examined. Fluorescence studies also demonstrated that BF227 bound to Lewy bodies, as indicated by the co-localisation of BF227 staining with α-synuclein-positive Lewy bodies (Fig. 3). Noteworthy, the concentration of BF227 used for the fluorescent studies was considerably higher (100 μM) that the low nanomolar concentrations typically achieved during in vivo PET studies (Kudo et al., 2007).

In conclusion this study supports the notion that [^{18}F]-BF227 is not entirely selective for Aβ pathology. Whilst previous PET studies were conducted using the carbon-11 labelled BF227, we anticipate that our results would be applicable to both [^{11}C]- and [^{18}F]-labelled BF227 PET studies, as the chemical nature of BF227 is not altered using either radioisotope. Therefore, taking into consideration the calculated K_D for α-synuclein fibrils and the size and cortical density of Lewy bodies, we speculate that the potential contribution of Lewy bodies to [^{11}C]-BF227-PET retention in the brains of Alzheimer's disease and even dementia with Lewy bodies patients (when assessed), should be considered to be extremely low. Nevertheless, given the high affinity for α-synuclein, added to the high density of Lewy bodies in the substantia nigra of most Parkinson's disease patients, evaluation of BF227 as a Parkinson's disease diagnostic biomarker, does warrant further investigation.

Acknowledgments

The authors would like to thank Prof. Catriona McLean, Fairlie Hinton and Geoff Pavey from the National Neural Tissue Resource

Centre for sourcing and preparation of the human brain tissue. We acknowledge the funding from the National Health and Medical Research Council and Ministry of Health, Labour and Welfare, Japan. RC is an NHMRC Senior Research Fellow.

References

Agdeppa, E.D., Kepe, V., Liu, J., Flores-Torres, S., Satyamurthy, N., Petric, A., Cole, G.M., Small, G.W., Huang, S.C., Barrio, J.R., 2001. Binding characteristics of radiofluorinated 6-dialkylamino-2-naphthylethylidene derivatives as positron emission tomography imaging probes for beta-amyloid plaques in Alzheimer's disease. J. Neurosci. 21, RC189.

Boxer, A.L., Rabinovici, G.D., Kepe, V., Goldman, J., Furst, A.J., Huang, S.C., Baker, S.L., O'Neil, J.P., Chui, H., Geschwind, M.D., Small, G.W., Barrio, J.R., Jagust, W., Miller, B.L., 2007. Amyloid imaging in distinguishing atypical prion disease from Alzheimer disease. Neurology 69, 283–290.

Braak, H., Del Tredici, K., Rub, U., de Vos, R.A., Jansen Steur, E.N., Braak, E., 2003. Staging of brain pathology related to sporadic Parkinson's disease. Neurobiol Aging 24, 197–211.

Bresjanac, M., Smid, L.M., Vovko, T.D., Petric, A., Barrio, J.R., Popovic, M., 2003. Molecular-imaging probe 2-(1-[6-[(2-fluoroethyl)(methyl) amino]-2-naphthyl]ethylidene) malononitrile labels prion plaques in vitro. J Neurosci 23, 8029–8033.

Cappai, R., Leck, S.L., Tew, D.J., Williamson, N.A., Smith, D.P., Galatis, D., Sharples, R.A., Curtain, C.C., Ali, F.E., Cherny, R.A., Culvenor, J.G., Bottomley, S.P., Masters, C.L., Barnham, K.J., Hill, A.F., 2005. Dopamine promotes alpha-synuclein aggregation into SDS-resistant soluble oligomers via a distinct folding pathway. FASEB. J. 19, 1377–1379.

Culvenor, J.G., McLean, C.A., Cutt, S., Campbell, B.C., Maher, F., Jakala, P., Hartmann, T., Beyreuther, K., Masters, C.L., Li, Q.X., 1999. Non-Abeta component of Alzheimer's disease amyloid (NAC) revisited. NAC and alpha-synuclein are not associated with Abeta amyloid. Am. J. Pathol. 155, 1173–1181.

Fodero-Tavoletti, M.T., Smith, D.P., McLean, C.A., Adlard, P.A., Barnham, K.J., Foster, L.E., Leone, L., Perez, K., Cortes, M., Culvenor, J.G., Li, Q.X., Laughton, K.M., Rowe, C.C., Masters, C.L., Cappai, R., Villemagne, V.L., 2007. In vitro characterization of Pittsburgh compound-B binding to Lewy bodies. J. Neurosci. 27, 10365–10371.

Forno, L.S., 1996. Neuropathology of Parkinson's disease. J. Neuropathol. Exp. neurol. 55, 259–272.

Goedert, M., Spillantini, M.G., 2006. A century of Alzheimer's disease. Science. (New. York,. N.Y. 314, 777–781.

Klunk, W.E., Debnath, M.L., Pettegrew, J.W., 1995. Chrysamine-G binding to Alzheimer and control brain: autopsy study of a new amyloid probe. Neurobiol. Aging. 16, 541–548.

Klunk, W.E., Engler, H., Nordberg, A., Bacskai, B.J., Wang, Y., Price, J.C., Bergstrom, M., Hyman, B.T., Langstrom, B., Mathis, C.A., 2003. Imaging the pathology of Alzheimer's disease: amyloid-imaging with positron emission tomography. Neuroimaging Clinics of North America 13, 781-789, ix.

Klunk, W.E., Engler, H., Nordberg, A., Wang, Y., Blomqvist, G., Holt, D.P., Bergstrom, M., Savitcheva, I., Huang, G.F., Estrada, S., Ausen, B., Debnath, M.L., Barletta, J., Price, J.C., Sandell, J., Lopresti, B.J., Wall, A., Koivisto, P., Antoni, G., Mathis, C.A., Langstrom, B., 2004. Imaging brain amyloid in Alzheimer's disease with Pittsburgh compound-B. Ann. Neurol. 55, 306–319.

Klunk, W.E., Lopresti, B.J., Ikonomovic, M.D., Lefterov, I.M., Koldamova, R.P., Abrahamson, E.E., Debnath, M.L., Holt, D.P., Huang, G.F., Shao, L., DeKosky, S.T., Price, J.C., Mathis, C.A., 2005. Binding of the positron emission tomography tracer Pittsburgh compound-B reflects the amount of amyloid-beta in Alzheimer's disease brain but not in transgenic mouse brain. J. Neurosci. 25, 10598–10606.

Kudo, Y., Okamura, N., Furumoto, S., Tashiro, M., Furukawa, K., Maruyama, M., Itoh, M., Iwata, R., Yanai, K., Arai, H., 2007. 2-(2-[2-Dimethylaminothiazol-5-yl]ethenyl)-6-(2-[fluoro]ethoxy)benzoxazole: a novel PET agent for in vivo detection of dense amyloid plaques in Alzheimer's disease patients. J. Nucl. Med. 48, 553–561.

Mathis, C.A., Wang, Y., Holt, D.P., Huang, G.F., Debnath, M.L., Klunk, W.E., 2003. Synthesis and evaluation of 11C-labeled 6-substituted 2-arylbenzothiazoles as amyloid imaging agents. J. Medicinal. Chem. 46, 2740–2754.

McKeith, I.G., Dickson, D.W., Lowe, J., Emre, M., O'Brien, J.T., Feldman, H., Cummings, J., Duda, J.E., Lippa, C., Perry, E.K., Aarsland, D., Arai, H., Ballard, C.G., Boeve, B., Burn, D.J., Costa, D., Del Ser, T., Dubois, B., Galasko, D., Gauthier, S., Goetz, C.G., Gomez-Tortosa, E., Halliday, G., Hansen, L.A., Hardy, J., Iwatsubo, T., Kalaria, R.N., Kaufer, D., Kenny, R.A., Korczyn, A., Kosaka, K., Lee, V.M., Lees, A., Litvan, I., Londos, E., Lopez, O.L., Minoshima, S., Mizuno, Y., Molina, J.A., Mukaetova-Ladinska, E.B., Pasquier, F., Perry, R.H., Schulz, J.B., Trojanowski, J.Q., Yamada, M., 2005. Diagnosis and management of dementia with Lewy bodies: third report of the DLB Consortium. Neurology 65, 1863–1872.

McKeith, I.G., Galasko, D., Kosaka, K., Perry, E.K., Dickson, D.W., Hansen, L.A., Salmon, D.P., Lowe, J., Mirra, S.S., Byrne, E.J., Lennox, G., Quinn, N.P., Edwardson, J.A., Ince, P.G., Bergeron, C., Burns, A., Miller, B.L., Lovestone, S., Collerton, D., Jansen, E.N., Ballard, C., de Vos, R.A., Wilcock, G.K., Jellinger, K.A., Perry, R.H., 1996. Consensus guidelines for the clinical and pathologic diagnosis of dementia with Lewy bodies (DLB): report of the Consortium on DLB International Workshop. Neurology 47, 1113–1124.

Rowe, C.C., Ng, S., Ackermann, U., Gong, S.J., Pike, K., Savage, G., Cowie, T.F., Dickinson, K.L., Maruff, P., Darby, D., Smith, C., Woodward, M., Merory, J., Tochon-Danguy, H., O'Keefe, G., Klunk, W.E., Mathis, C.A., Price, J.C., Masters, C.L., Villemagne, V.L., 2007. Imaging beta-amyloid burden in aging and dementia. Neurology 68, 1718–1725.

Trojanowski, J.Q., 2002. Emerging Alzheimer's disease therapies: focusing on the future. Neurobiol. Aging. 23, 985–990.

社団法人 電子情報通信学会
THE INSTITUTE OF ELECTRONICS,
INFORMATION AND COMMUNICATION ENGINEERS

信学技報
IEICE Technical Report

1 計測信号参照系独立成分分析法のシミュレーション研究

幡谷速昭[1],木村芳孝[1],伊藤拓哉[1],辛島彰洋[1],片山統裕[1],八重樫伸生[1],中尾光之[1]

1 東北大学大学院情報科学研究科, 〒980-8579 宮城県仙台市青葉区荒巻字青葉 6-3-09

2 東北大学先端医工研究機構, 〒980-8575 宮城県仙台市青葉区星陵町 2-1

E-mail: 1:hataya@biomdl.ecei.tohoku.ac.jp, 2:ykimura@tubero.tohoku.ac.jp

あらまし Microsoft Word による電子情報通信学会技術研究報告形式のテンプレートファイルです.
キーワード Windows, Word, 信学技報, テンプレート

A simulation study of single-BSS with references

Toshiaki Hataya[1],Yoshitaka Kimura[1],Takuya Ito[1],Akihiro Karashima[1],Norihiro Katayama[1],

Nobuo Yaegashi[1],and Mitsuyuki Nakao[1]

1 Graduate School of Information Sciences, Tohoku University, 6-3-09, Aramaki-aza-aoba, Aoba-ku, Sendai, Miyagi-ken, 980-8579, Japan

2 Tohoku University Biomedical Engineering Research Organization, 2-1, seiryou-chou, Aoba-ku, Sendai, Miyagi-ken, 980-8575, Japan

E-mail: 1:hataya@biomdl.ecei.tohoku.ac.jp, 2:ykimura@tubero.tohoku.ac.jp

Abstract IEICE (The Institute of Electronics, Information and Communication Engineers) provides a word template file for the Technical Report of IEICE.
Keyword Windows, Word, Technical Report, Template

1. はじめに

技術研究報告の 1 ページ目上部には，タイトル，発表者氏名，所属，住所，メールアドレス，キーワードの和文と英文及びあらまし(和文 300 字程度，英文 100 語程度)を，それぞれ記述してください.

2. single-BSS with references

観測信号を $\mathbf{x}=(x_1,x_2,...,x_n)$ とする。この 1 本の信号から ICA を用いて複数の信号を得るためには次元を増やす処理が必要である。

まず、長さが N、間隔が τ の系列を抜き出す。これを時間を τ ずつずらして m 回行い、それらを結合することで、m×N の埋め込み行列 v を得る。

$$\mathbf{v}=\begin{pmatrix} x_t & x_{t+\tau} & \cdots & x_{t+N\tau} \\ x_{t+\tau} & x_{t+2\tau} & \cdots & x_{t+(N+1)\tau} \\ \vdots & \vdots & \ddots & \vdots \\ x_{t+(m-1)\tau} & x_{t+m\tau} & \cdots & x_{t+(m+N-1)\tau} \end{pmatrix}$$

(m：次元, N：信号の長さ, τ ：ずらし幅)

参照信号 r は、行列 v の 1 行目にバンドパスフィルタをかけたときの応答を用いる。

以上のようにして得られた行列 v と参照信号 r を用いて参照信号付きブラインド信号分離(BSSR)を行い、複数の信号を得る。

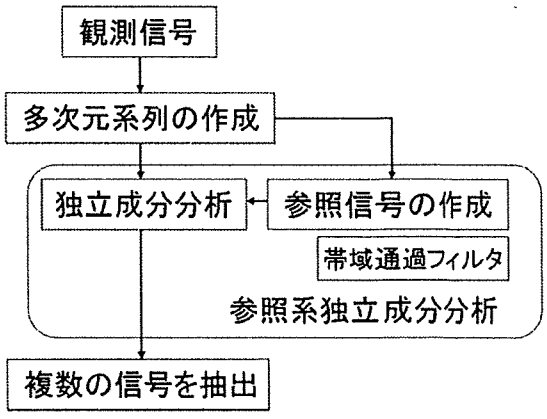

図 1 single-BSS with References の流れ

3. シミュレーション

3.1. 信号の準備

観測信号 x として以下の信号を用い(図 2)、この信号

から m=31, τ =1 の埋め込み行列 v を作成した。サンプリングレートは 1000Hz である。

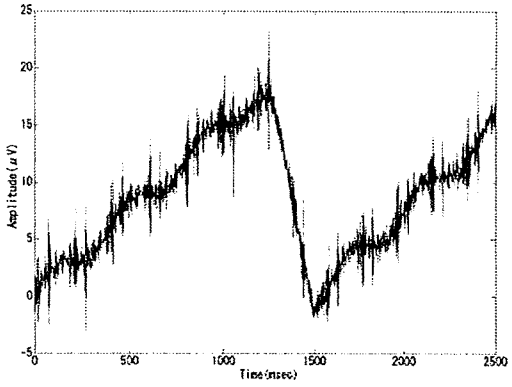

図 2　観測信号 x

参照信号は 3 つ用意した(図 3)。作成に用いたバンドパスフィルタの通過帯域はそれぞれ以下の通り。

r_1 : 0.1～1.0Hz

r_2 : 5～498Hz

r_3 : 1～5Hz

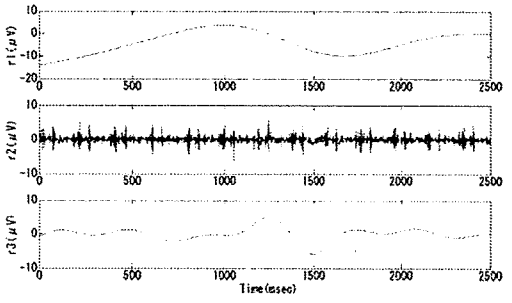

図 3　参照信号

BSSR を行い、チャンネル 1～3 で得られた信号を以下に示す(図 4)。1 つの観測信号から 3 つの異なる成分が分離できている。

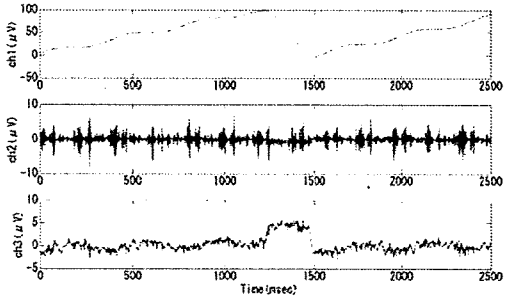

図 4　分離信号

これら 3 つの信号を上からソース信号 s_1,s_2,s_3 とし、適当な行列 $A=\begin{pmatrix}0.2 & 0.6 & 0\end{pmatrix}^T$ で混合したものを、以降のシミュレーションの観測行列 x として用いる。

3.2. 分離条件

m=31, τ =1 の場合においては図 4 のように 3 つの異なる成分が分離できた。以降、次のような条件でシミュレーションを行い、得られる信号について調べる。

(1)次元数 m を変化させる。

(2)ずらし幅 τ を変化させる。

4. 結果

4.1. 次元数 m を変化させた場合

τ =1 の場合において m=5 から m=100 まで変化させて分離を行った。参照信号の作り方は先程と同様である。結果を図 5,6 に示す。

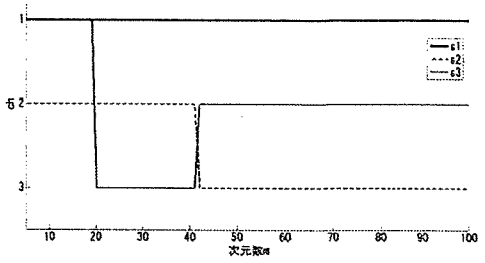

図 5　信号の出現チャンネル

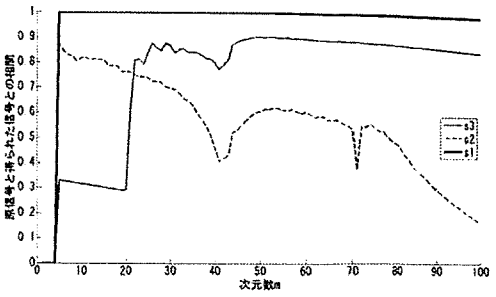

図 6　原信号と得られた信号との相関係数

図 5,6 より、3 つの信号が分離できたのは m≧20 のときで、m=41,42 の間で s2,s3 の出現チャンネルが入れ替わっており、そこで分離精度が落ち込んでいる。s1 は m の値に関らず分離精度が高い。s2 は m の増加とともに分離精度が落ちている。

以下に m=10(図 7),m=31(図 8),m=100(図 9)の場合の分離結果を示す。

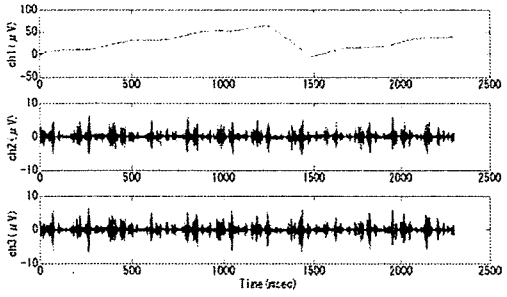

図 7　m=10 の場合の分離結果

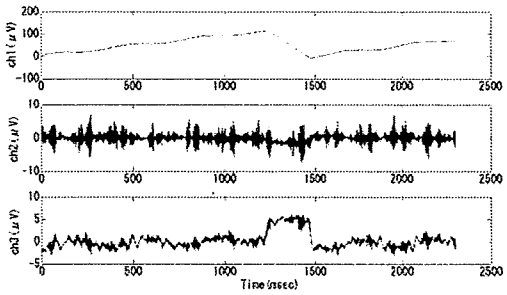

図 8　m=31 の場合の分離結果

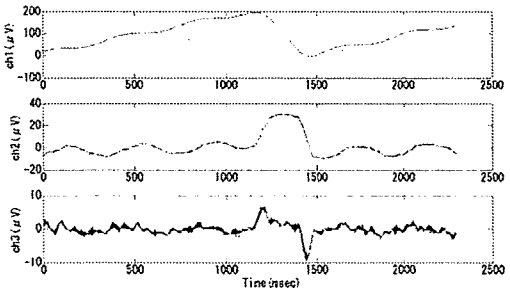

図 9　m=100 の場合の分離結果

図 7,8,9 を見ると、m=10 の場合は s3 が見えていない。m=100 の場合は ch3 にどの原信号とも異なる信号が現れている。m≧20 の場合に得られた信号と原信号との時間のずれを図 10 に示す。

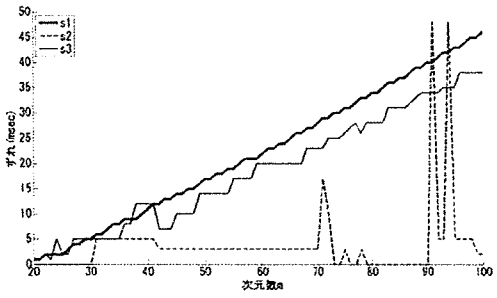

図 10　得られた信号と原信号との時間のずれ

s1,s3 のずれは次元数 m に比例しているように見える。s2 のずれは m=71,91,94 の場合を除けば、m の変化に関らずほぼ一定である。

4.2. ずらし幅 τ を変化させた場合

m=31 の場合において τ=1 から τ=10 まで変化させて分離を行った。

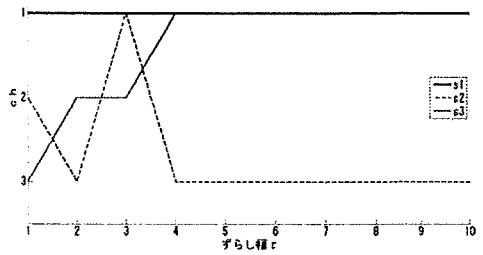

図 11　信号の出現チャンネル

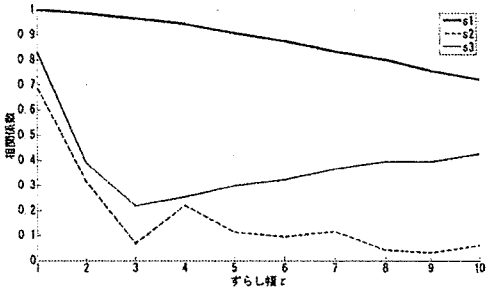

図 12　原信号と得られた信号との相関係数

3 つの信号が分離できたのは τ=1,2 の場合だけだった。相関係数は τ=1 の場合が最も高く、それ以外では s1 以外の信号は分離できなかった。τ=2 の場合の分離信号を図 13 に示す。

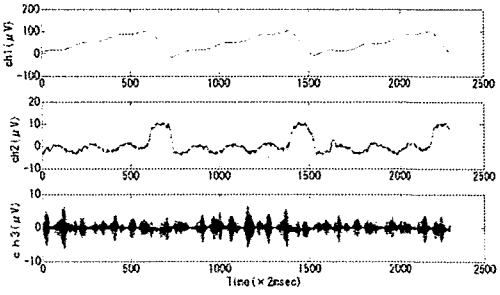

図 13　τ=2 の場合の分離結果

4.3.

5. 結論

m と τ を変化させると各信号はそれぞれ異なる振る舞いをした。次元数 m を増やしても分離精度は必ずしも向上するわけではなく、時間のずれ方も各信号で異

なっていることから、信号の種類によって適切なmの範囲が存在するのは間違いないと思われる。

文　献

[1] (雑誌の場合) 著者名, "標題," 雑誌名, 巻, 号, pp.を付けて始め－終りのページ, 月(英語)年.

[2] (雑誌例 1) 山上一郎, 山下二郎, "パラメトリック増幅器, "信学論(B), vol.J62-B, no.1, pp.20-27, Jan.1979.

[3] (雑誌例 2) W. Rice, A. C. Wine, and B. D. Grain, diffusion of impurities during epitaxy, Proc. IEEE, vol.52, no.3, pp.284-290, March 1964.

[4] (著書, 編書の場合) 著者名, 書名, 編者名, 発行所, 発行都市名, 発行年.

[5] (著書, 編書例 1) 山田太郎, 移動通信, 木村次郎(編), pp.21-41, (社) 電子情報通信学会, 東京, 1989.

[6] (著書, 編書例 2) H. Tong, Nonlinear Time Series: A Dynamical System Approach, J. B. Elsner, ed., Oxford University Press, Oxford, 1990.

[7] (著書の一部を引用する場合) 著者名, "標題, "書名, 編者名, 章番号または pp.を付けて始め－終りのページ, 発行所, 発行都市名, 発行年.

母体葉酸欠乏が胎仔胎盤発育に及ぼす影響と そのエピジェネティック制御機構解析

東北大学大学院医学系研究科医科学専攻
発生・発達医学講座周産期医学分野
松田　尚美

目　次

Ⅰ．要約

【目的】「Developmental Origins of Health and Disease 説（Fetal Programming）」が、近年の疫学的研究により広く支持され注目されている。ヒストン修飾や DNA メチル化などのエピジェネティクスが、その中心的役割を担っていると考えられるが、その詳細な機序は未だ不明である。メチル基のドナーであり多様なエピジェネティック経路に関わる葉酸が Fetal Programming に関わるのではないかと考え、“葉酸欠乏マウスモデル”を作製し、胎仔胎盤発育における葉酸のエピジェネティック制御機構の解明を目指した。
【方法】妊娠マウスを、妊娠全期間通常餌で飼育した C 群、妊娠前半期を通常餌、妊娠後半期を葉酸を含まない葉酸欠乏餌で飼育した FD(8-17)群、妊娠全期間葉酸欠乏餌で飼育した FD(0-17)群、妊娠前半期を通常餌、妊娠後半期をタンパク制限餌で飼育した PR(8-17)群の 4 群に分類し、リアルタイム RT-PCR 法を用いて遺伝子発現解析を行った。さらに、クロマチン免疫沈降法・バイサルファイトシークエンス法を用いて遺伝子発現変化の背景にあるエピジェネティック解析を行った。
【結果】FD(8-17)群メスでは有意に胎仔体重と胎盤重量の減少を認めた。FD(8-17)群オス胎盤では有意な *Igf2 (Insulin-like growth factor 2)* の上昇、*Igfbp1(Insulin-like growth factor binding protein 1)* の低下を認めた。さらに *Igf2* のプロモーター領域では H3K4-me3, H3K9-me3 によるヒストン活性変化がおこっていた。胎仔脳では、*Hdac7a(Histone deacetylase 7a)*、*Folr1(Folate receptor 1)* の遺伝子発現変化が認められ、さらにそれらのプロモーター領域では H3K9-Ac, H3K4-me3 によるヒストン活性変化がおこっていた。また、メスでのみ発現変化をおこした遺伝子群 *Bmp2 (Bone morphogenetic protein)*, *Cckbr (Cholecystokinin B receptor)*, *Mc2r (Melanocortin 2 receptor)*などは生活習慣病関連遺伝子群であった。
【考察】妊娠後半期の葉酸欠乏により、特にメスにおいて胎仔と胎盤の発育が制限されることがわかった。オスではその発育制限が有意でなかったのは、Igf-axis の制御によるものと考えられた。その背景にはプロモーター領域のヒストン修飾の変化が関連していると考えられ、胎盤において葉酸欠乏によりエピジェネティック変化が生じていることが示唆された。また、胎仔脳における *Hdac7a*、*Bmp2*、*Folr1* の発現変化、*Bmp2*、*Folr1* のプロモーター領域でのヒストン活性化の解析から、母体葉酸欠乏により胎仔脳においてもエピジェネティック変化が生じていることが示唆された。さらに、妊娠後半期葉酸欠乏のメスにおいては、生活習慣病関連遺伝子に発現変化が顕著であり、メスにおいて生活習慣病のリスクが高くなることが示唆された。
【結論】母体葉酸欠乏は子宮内胎児発育不全を惹起し、またエピジェネティック変化を引き起こして胎児に生涯にわたる影響を及ぼしていることが示された。
また、母体葉酸欠乏による胎仔への影響には性差があり、オスよりもメスのほうが葉酸欠乏のストレス・影響を受けやすいことが示唆された。

Ⅱ. 研究背景

「胎児期において、感受期に器官や臓器に対して侵襲やストレスが加わると将来の疾病の発生や健康状態に影響を及ぼす」という“成人病胎児期発症説 Fetal Origins of Adult Disease (FOAD)”は“胎児プログラミング仮説”、“Barker 説”とも呼ばれ、「さまざまな成人期慢性疾患の発症基盤が受胎前後、胎芽期、胎児期、出生後の環境と関連する」という“Developmental Origins of Health and Disease(DOHaD)説”に展開し、現在周産期医療において重要な概念となりつつある。1980 年代、Barker らは、疫学研究を基に、胎児発育が抑制され不可逆的な組織や機能の変化が生じること（programming）が、成人期の心血管系疾患や 2 型糖尿病のリスクになると考えた。1986 年、“胎児が子宮内で低栄養に曝露されたとき、体重を増やさないようにし（結果的に子宮内胎児発育不全となり低出生体重児となる)、インスリン抵抗性をもつことが出生後の飢餓に備えるための適応である”として”thrifty phenotype（倹約表現型）“仮説を提唱し、これによって胎児期に生活習慣病の起源を獲得するのではないかと推測した。

一方、Neel らは、“何万年もの間人類は狩猟生活を経て飢餓状態に適応できるような thrifty genotype を獲得しており、そのため近代化が急速に進み豊かになる地域に 2 型糖尿病が増加するのではないか”という”thrifty genotype（倹約遺伝子）”仮説を提唱している。なお彼らのいう倹約遺伝子とは架空の遺伝子であり、現時点で明らかにされているものではない。いずれにしても、これらの仮説では、栄養摂取が制限されているのならば健康に過ごせるが、豊富な栄養環境では疾病発症につながることになる。さらに 2004 年、Gluckman と Hanson は、“発達期の環境の変化に対応した不可逆的な反応（developmental plasticity）が生じると、発達が完了した時期の環境とマッチすれば健康に生活できるが、もしマッチしなければ成人期のさまざまな疾患の源になる”という考え方を提唱した。さらにこのような研究を通じてヒトの健康についての公衆衛生学的な啓蒙、あるいは疾病予防に資することも意図して、Developmental Origins of Health and Disease(DOHaD)という用語が使われるようになった。Gluckman と Hanson は、感受期における環境要因の内容や程度によって、ヒトはさまざまな変化を示し、極端な場合は developmental disruption（例として葉酸欠乏による神経管開存症など。）となり、また生存と引き換えに子宮内胎児発育不全や早産となる場合（trade-off、coping、immediately adaptive response などという。）や、子宮内胎児発育不全とはならなくても発達完了期の環境を予測するかのように内分泌・代謝などの反応性が変化（predictive adaptive responses）するのではないかと考えた。DOHaD の概念は、メタボリックシンドロームのみならずさまざまな成人期の慢性疾患との関連性を説明する上で都合が良いとされる。出生前・後の環境によって変化がもたらされる時期は各臓器や器官で一定ではなく、その反応も一様ではない。Developmental disruption を除けば、これらの反応は発達期の環境に適応したものであるがゆえに意味をなすものであって、各臓器・器官の発達が完了する頃の環境とそぐわない（ミスマッチ）場合に、健康への影響が出現することになる。

DOHaD は発達期の環境に応じて個体に developmental plasiticity が起こることを起源としている。環境によってもたらされるヒトへの影響を決定するのは遺伝子と環境の相互作用であり、その本態を説明する上でエピジェネティクスの概念は欠かせないものである。developmental plasiticity は、環境によって DNA 配列変化を伴わず子孫へと伝達される遺伝子機能の変化（エピジェネティック変化）によってもたらされた状態であると考えられている。

“遺伝子 DNA の塩基配列に変化がなくても遺伝子機能が損なわれるメカニズムであるエピジェネティクス“を変化させ得る環境要因として、栄養がそのひとつと考えられる。母体の栄養状態が出生後の児の健康に何らかの影響を及ぼすとの疫学研究の最初の報告は、1976 年の Ravelli らによるものであり、妊娠中低栄養の最大の人体実験モデルとなってしまった Dutch famine では、子宮内で低栄養に暴露された児は成人後に高頻度に肥満を呈したとされる(1)。 その後 1987 年に Barker らが胎生期の低栄養が成人後の肥満・耐糖能

異常・高血圧などを高率に発症させ、心血管障害による死亡率を上昇させるとする疫学的報告を行い「Barker theory」として注目され(2)、この現象は胎生期の劣悪な子宮内環境に対して発達中の胎児臓器が適応し、その適応が生涯刻み込まれるとされる「Fetal progrraming」と呼ばれている(3)。その後、母体低栄養研究はタンパク質制限動物モデルなどでさかんに行われ、母体タンパク質制限は、児に高血圧(4)・耐糖能異常・血管内皮機能異常(5)を引き起こすことなどが報告されている。タンパク質だけではなく、ビタミン群も正常な成長発達に不可欠であると考えられ、特に、葉酸はメチルドナーとして知られており、DNAサイクルに関連する栄養因子のひとつであり、その摂取の良否はダイレクトにエピジェネティックな遺伝子調節機構に影響を及ぼすのではないかと考えられる(6,7,8,9)。 葉酸は、1941 年に乳酸菌の増殖因子としてホウレンソウの葉から発見された水溶性ビタミンであり、ビタミン B 群のひとつである。別名、ビタミン M, ビタミン B9、プテロイルグルタミン酸とも呼ばれる。テトラヒドロ葉酸（葉酸の誘導体）は、核酸・アミノ酸の代謝に用いられる。葉酸は細胞の増殖に関わる非常に重要な栄養素であり、細胞の中で、ホモシステインをメチオニンに変換するときにテトラヒドロ葉酸を必要とする。特に妊娠中は胎児の発育に伴って細胞増殖が活発になるため、葉酸の要求量が増大するのである。そのために、妊娠週数が進むにつれて、血清中の葉酸値が低下すると言われている。

1999 年 Piedrahita らにより葉酸受容体ノックアウトマウスでは神経管閉鎖障害が生じ、また妊娠 10 日目までに子宮内胎仔死亡になることが報告され(10,11) 、2002 年に Burgoon らにより、葉酸欠乏餌を与えた妊娠マウスでは胎仔体重の減少や流産率の増加、口蓋裂や心奇形が増加することが報告されている(10,12,13)。 2003 年、Waterland らは妊娠マウスにメチル化基質を投与した結果、新生仔の DNA の特有部分においてメチル化が強化されていることを報告し(7)、生活習慣病とのかかわりについて述べた(8)。また、2005 年、Lillycrop らは新生仔の遺伝子のメチル化について調べ、低栄養環境下の妊娠ラットから生まれた新生仔ではメチル化が低下して異常に高い発現を認め、低栄養だが葉酸補充を受けた妊娠ラットから生まれた新生仔ではメチル化が回復して正常発現レベルに復していることを報告した(9)。葉酸欠乏が神経管閉鎖障害をはじめとする奇形を引き起こすことについては、現在までに多くの研究がなされ、1992 年にはアメリカ CDC により妊娠可能女性に葉酸摂取を推奨する勧告が出され、2000 年には日本でも厚生省より同様に妊娠前から葉酸を 0.4mg/日摂取することを推奨する勧告が出されており、コンセンサスが得られている。しかしながら依然として、葉酸が奇形以外に胎児胎盤発育に及ぼす影響、さらには葉酸が胎児に及ぼすエピジェネティック変化の影響については未だ解明されていないのが現状である。母体葉酸欠乏の器官発生異常に対する影響については、神経管開存症に代表されるように妊娠初期の欠乏が高リスク群であるが、これについてはすでに多くの研究結果が発表されている。従って本研究では特に妊娠後期における母体葉酸欠乏が及ぼす、胎盤及び胎仔の発育異常に注目した。

第二次世界大戦時のオランダ飢饉（Dutch famine）の際、低栄養妊婦から出生した児は低出生体重児が多く、また成人後の生活習慣病の発症が多かったという疫学調査が、現在の DOHaD 概念の基となっている。これが現在わが国で再びクローズアップされている理由は、新生児の出生体重の平均値が 1970 年代より減少の一途をたどってきたからである。これは先進国にあっては特異な状況である。平均出生体重の低下の原因については、出産年齢女性の痩せ願望による BMI の低下や、妊娠中の一律の体重増加制限などが挙げられているが、このことは、生活スタイルの欧米化とあいまって、わが国における生活習慣病をはじめとするさまざまな疾患の増加が危惧される。

本研究においては、以上の観点から、母体葉酸欠乏による胎仔胎盤発育への影響を解析し、また、母体葉酸欠乏による胎仔胎盤における葉酸のエピジェネティック制御機構を解析する。